

# Implementation of a new crop and irrigation scheme in the ISBA land surface model using SURFEX\_v8.1

Arsène Druel<sup>1,2</sup>, Simon Munier<sup>1</sup>, Anthony Mucia<sup>1</sup>, Clément Albergel<sup>1,3</sup> and Jean-Christophe Calvet<sup>1</sup>

<sup>1</sup>CNRM, Université de Toulouse, Météo-France, CNRS, Toulouse, France

5 <sup>2</sup>Now at Ecologie des Forêts Méditerranéennes (URFM), Institut national de recherche pour l'agriculture, l'alimentation et l'environnement (INRAE), Avignon, France

<sup>3</sup>Now at European Space Agency Climate Office, ECSAT, Harwell Campus, OX11 0FD Didcot, Oxfordshire, United Kingdom

10 *Correspondence to:* Jean-Christophe Calvet (jean-christophe.calvet@meteo.fr), Arsène Druel (arsene.drue@umr-cnrm.fr)

**Abstract.** With an increase in the number of natural processes represented, global land surface models (LSMs) have become more and more accurate in representing natural terrestrial ecosystems. However, they are still limited with respect to the impact of agriculture on land surface variables. This is particularly true for agro-hydrological processes related to a strong human control on freshwater. While  
15 most LSMs consider natural processes only, the development of human-related processes, e.g. crop phenology and irrigation in LSMs, is key. In this study we present the implementation of a new crop and irrigation scheme in the ISBA (Interaction between Soil, Biosphere, and Atmosphere) LSM. This highly flexible scheme is designed to account for various configurations and can be applied at different spatial scales. For each vegetation type within a model grid cell, three irrigation systems can be used at  
20 the same time. A limited number of parameters are used to control (1) the amount of water used for irrigation, (2) irrigation triggering (based on the soil moisture stress) and (3) crop seasonality (emergence, harvesting). A case study is presented over Nebraska (USA). This region is chosen for its high irrigation density and because independent observations of irrigation practices can be used to verify the simulated irrigation amounts. The ISBA simulations with and without the new crop  
25 phenology and irrigation scheme are compared to different satellite-based observations. The comparison shows that the irrigation scheme improves the simulated vegetation variables such as leaf area index and gross primary productivity and other variables largely impacted by irrigation such as evapotranspiration and land surface temperature. In addition to a better representation of land surface processes, the results

point to potential applications of this new version of the ISBA model for water resource monitoring and  
30 climate change impact studies.

## 1 Introduction

Amongst the global water withdrawal from rivers, reservoirs and groundwater, the share used for agriculture is estimated to reach 69 % on average, with some regional heterogeneity - over 90 % in some regions (Hoekstra and Mekonnen, 2012, FAO, 2014). This amount of water is likely to increase in  
35 the future in relation to climate warming and population growth (United Nations et al., 2019, Field et al., 2014). Future irrigation needs will likely be stronger in Africa. Now, only 5 % of cultivated land is under irrigation in Africa, against 21 % at a global scale (FAO, 2014). The historical evolution of irrigation also points to increasing water consumption: the area equipped for irrigation nearly doubled from 1900 to 1950, when it tripled from 1950 to 2005 (Siebert et al., 2015).

40 Irrigation is used to increase crop yields by controlling the soil water stress (Fraiture et al., 2007). Several studies indicate that yields can be higher by a factor of two or more when the fields are irrigated (Bruinsma, 2009; Colaizzi et al., 2009; Siebert and Döll, 2010; FAO, 2014). However, freshwater is already a limited resource and the current evolution of irrigation has a substantial impact on: (1) river discharge, with a decrease in their lower reaches due to diversions and impoundments for  
45 irrigation (Tang et al., 2008; Piao et al., 2010; Grafton et al., 2018), (2) groundwater level, with critical low levels observed in case of intensive irrigation (Rodell et al., 2009; Döll et al., 2012; Pfeiffer and Lin, 2014), (3) the surface energy budget through an increase of evapotranspiration, which can lead to surface cooling (Kueppers et al., 2007; Lobell et al., 2008; Jiang et al., 2014; de Vrese et al., 2016). Water vapour originating from large scale irrigation water supply can be recycled to rainfall and affect  
50 non-irrigated areas (Moore and Rojstaczer, 2002; DeAngelis et al., 2010; Carrillo-Guerrero et al., 2013; Harding et al., 2013). It can also affect the dynamics of the monsoon (Douglas et al., 2006; Saeed et al., 2009; Shukla et al., 2014) and influence climate at both regional and global scales (Sacks et al., 2009; Puma and Cook, 2010). These findings show a gradual and significant influence of changes in irrigated areas on the hydrological cycle (e.g. Adegoke et al., 2003; Haddeland et al., 2006; Rost et al., 2008;

55 Döll et al., 2009; Hanasaki et al., 2010; Biemans et al., 2011). The ability of numerical models to reproduce these different impacts and feedbacks is thus essential in order to understand the role of irrigation in the Earth climate system at different spatial scales (Zaitchik et al., 2005). Representing irrigation could potentially improve weather and climate forecast skill (Ozdogan et al., 2010). However, as presented below, irrigation is generally represented in models in a too simplistic way.

60 Land surface models (LSMs) represent land surface biophysical processes and variables, including soil moisture and vegetation biomass, in a way that is fully consistent with the representation of carbon, water and energy fluxes. However, current models have to improve the representation of anthropogenic factors and their interactions with natural processes (Verburg et al., 2016). In particular, LSMs need to represent the complexity of irrigation practices as much as possible, and their impact on  
65 the environment. Efforts are made to achieve this goal in the Community Land Model (CLM) and Noah-MP LSMs (Felfelani et al. 2020, Zhang et al. 2020, respectively). However, as highlighted by Chukalla et al. (2015), many large scale LSMs currently represent only one type of irrigated vegetation (mostly C4 crops, i.e. crops with a C4 photosynthesis carbon fixation type, such as corn, sorghum), with only one type of irrigation practice (e.g. sprinkling or flooding), one season per year and no inter-annual  
70 variability of vegetation density (Perry, 2007; Perry et al., 2009). Among others, this is the case in the current version of the ISBA (Interaction between Soil, Biosphere, and Atmosphere; Noilhan and Planton, 1989) LSM, with C4 crops irrigated with sprinkling (Voirin-Morel, 2003; Calvet et al., 2008). In reality, there are a lot of different vegetation types which can be irrigated, from orchards to pastures (FAO, 2014), and different irrigation techniques with different ways to apply water (above the  
75 vegetation or directly on the ground for sprinkling and flooding irrigation techniques, respectively). Different irrigation types vary in (1) irrigation efficiency (Evans and Sadler, 2008; Jägermeyr et al., 2015), (2) the amount of freshwater used for irrigation per surface unit (FAO, 2014), and (3) impact on water resources (Khan and Abbas, 2007). Moreover, some specificities of irrigation such as the timing and frequency of water application can affect the ecosystem and atmospheric responses to irrigation  
80 (Sorooshian et al., 2012). Some models include a representation of irrigation without having an interactive vegetation scheme and using climatological values instead (such as with the LIS-Noah

model, a NASA land information system and LSM combination, used in Lawston et al., 2015), thereby precluding inter-annual variability of vegetation density and the impact of irrigation on vegetation growth. Having a more complete irrigation description is needed to reproduce the irrigation seasonality, and to represent possible changes in crop phenology such as emergence and harvest dates. The impact of changing irrigation characteristics in a context of climate change could thereby be evaluated, such as increasing irrigation efficiency (currently around 56%; FAO, 2014) and freshwater saving potential (Perry et al., 2017; Koech and Langat, 2018).

The objective of this work is to develop and evaluate a more detailed representation of irrigation practices into the ISBA LSM within the SURFEX (SURFace EXternalisée) modelling platform (Masson et al., 2013).

Section 2 presents a description of the ISBA LSM, the new crop and irrigation scheme, the validation protocol, followed by a description of the observational datasets. Section 3 illustrates the impact of the new scheme when compared to simulations without crop phenology and without irrigation. An evaluation of the performance of the model is made over Nebraska. Section 4 discusses the added value and the limits of the newly implemented irrigation scheme. Finally, section 5 presents the conclusions and future research directions.

## **2 Materials and Methods**

### **2.1 The ISBA land surface model**

The ISBA model (originally described in Noilhan and Planton, 1989) is the LSM developed by the research department of Météo-France (Centre National de Recherches Météorologiques, CNRM). It is embedded into the SURFEX modelling platform (Masson et al., 2013; Voldoire et al., 2017; Le Moigne et al., 2018), and can provide initial land surface conditions to various atmospheric models (e.g. ALADIN in Fischer et al., 2005), or be forced by atmospheric conditions in offline (i.e. stand-alone) mode. SURFEX integrates different models describing ocean and terrestrial surfaces. Over land, specific models are used to represent water bodies, cities, and the soil-plant system. The latter is modelled by the ISBA LSM. In SURFEX, land cover is described by ECOCLIMAP-II (Faroux et al.,

2013). This study takes advantage of the ECOCLIMAP-SG (Calvet and Champeaux, 2020; Supplement S1) major update of ECOCLIMAP-II. The ISBA model can be coupled to the CTRIP model (Decharme et al., 2019, Munier and Decharme, 2021) which is specifically designed to represent water dynamics within rivers and aquifers. The SURFEX framework allows the coupling of terrestrial processes with atmospheric models and hydrological models. For agricultural drought and water resource monitoring, SURFEX can also be operated offline, forced by a pre-existing dataset of atmospheric variables. Only offline ISBA simulations are considered in this study. In SURFEX, the evolution of land surface states (surface temperature, albedo, roughness...) and fluxes (evaporation, sensible heat flux, ground heat flux, net ecosystem exchange of CO<sub>2</sub>) is simulated for four different tiles: natural and cultivated lands (e.g. deciduous and broadleaf forests, tropical, temperate and boreal grasslands, crops, deserts, ...), urban areas, oceans and inland waters (such as lakes). The ISBA LSM is used to simulate natural and cultivated lands.

In this study, the version of ISBA including photosynthesis and temporal dynamical LAI evolution in response to environmental conditions is used (ISBA-A-gs; Calvet et al., 1998; Gibelin et al., 2006), together with the multi-layer soil hydrology scheme described in Decharme et al. (2019). Phenology is entirely driven by photosynthesis and no growing degree-day model is used. The only phenology parameter is a minimum LAI value, of 0.3 m<sup>2</sup>m<sup>-2</sup> for low vegetation. The SURFEX v8.1 version (Le Moigne et al., 2018) is used to do the simulations. Since this study focuses on irrigation, only the tile of natural and cultivated lands is simulated with ISBA, representing the evolution of soil (temperature and water profiles), vegetation (leaf-level and canopy-level photosynthesis, biomass, LAI and carbon fluxes), surface hydrology (runoff and drainage) and snow conditions. To represent the global-scale diversity of continental natural surfaces, twenty different surface types (hereafter referred to as “nature types”) can be used in ECOCLIMAP-SG (see Fig. S1.1 and Table S1.2).

## 2.2 Irrigation modelling concept

In this study, a pre-existing simple irrigation scheme (Calvet et al., 2008) within the ISBA LSM is upgraded to build a new version able to work at a global scale and to represent several types of irrigation practices. The irrigation can be activated for ISBA versions able to simulate interactive

135 vegetation biomass and LAI. Sprinkler irrigation is represented by imposing an additional water flux forcing to the soil-plant system. Water is applied at a given time and over a certain period of time. A number of irrigation parameters need to be assigned such as the irrigation amount, the irrigation interval, the irrigation start and end times. A parsimonious approach is used in order to limit the number of parameters of the model. Table 1 lists the parameters and the values used by default in the model.

140 Using these values allows the model to predict a realistic amount of irrigation water over irrigated corn in southern France (Bonnemort et al., 1996; Voirin-Morel, 2003; Calvet et al., 2008). Irrigation is triggered using thresholds of the simulated extractable soil moisture content, when vegetation growth is limited by a soil moisture deficit. The plant water stress level is evaluated using a unitless soil wetness index along the root profile ( $SWI_{root\_zone}$ ). A  $SWI_{root\_zone}$  value close to one corresponds to a well-

145 watered soil, while a value close to zero indicates extreme stress. In order to trigger irrigation, the  $SWI_{root\_zone}$  value is compared to predefined SWI thresholds given as input parameters. These SWI thresholds are evolving during the irrigation season and default values are fixed to 0.7 for the first irrigation, 0.55 for the second irrigation, 0.4 for the third irrigation, and 0.25 afterwards. This irrigation strategy tends to limit water applications when the plant is able to extract water from the soil. When a

150 SWI threshold is reached, irrigation is triggered with a predefined quantity of water of 30 mm (by default), following Calvet et al. (2008). The yearly sum of this irrigated water can be compared to the USGS data described in Section 2.4.3. The irrigation water flux is evenly distributed over a period of time of 8 hours (by default) and is applied on top of the vegetation canopy like precipitation. The irrigation water can be intercepted by vegetation canopy.

155 Moreover, specific crop phenology parameters such as emergence and harvest dates are used for irrigated crops. In practice, two dates are prescribed: emergence and harvest. This is a simple way to represent specific crop phenology attributes of irrigated crops. Between these two dates, irrigation is possible. Before the emergence and after the harvest, LAI is fixed at the model's minimum value ( $LAI = 0.3 \text{ m}^2 \text{ m}^{-2}$ ).

## 160 2.2.1 New irrigation processes

In Lawston et al. (2015), three irrigation types are considered: sprinkler irrigation, flood irrigation and drip irrigation. In the new version of ISBA the same irrigation types are represented but a different modelling approach is used. In this study, the sprinkler irrigation type is used and evaluated. Flood and drip irrigation will be considered in a future work. The new crop and irrigation algorithm is based on  
165 several steps described below and in Fig. 2.

Firstly, the model determines whether fields within the grid cell can be irrigated, i.e. they are equipped for irrigation (e.g. water supply, valves, pipes...). This information is given by the irrigation map described in section 2.4.1.

Secondly, the model checks that the vegetation growth stage is compatible with irrigation. For  
170 crops, irrigation can be triggered after the emergence and until a few days before the harvest (by default two weeks). The new crop and irrigation scheme provides the option to support up to three plant growth seasons per year. The crop phenology parameters are not applied to wooded vegetation (trees and shrubs), and can be applied without irrigation. Irrigation can optionally be triggered without considering any specific crop phenology parameter but this option is not considered in this study.

175 The availability of resources (equipment or local water distribution) is taken into account through a default minimum time gap between two successive irrigations (Zhang et al. 2019). This default irrigation interval parameter value is a constant (7 days by default) but maps of irrigation intervals could be used when available.

Since a multi-layer soil hydrology scheme is used in the new irrigation model, the root-zone  
180 SWI ( $SWI_{root\_zone}$ ) is a weighted average SWI value based on the soil volumetric water content profile ( $Wc_i$ ,  $m^3 m^{-3}$ ), the field capacity volumetric water content profile ( $Wfc_i$ ,  $m^3 m^{-3}$ ) and the wilting point profile ( $Wwilt_i$ , depending on clay and sand fraction,  $m^3 m^{-3}$ ), for each soil layer  $i$ . The root fraction inside each soil layer ( $f_{root_i}$ ) is used as a weighting factor:

$$SWI_{root\_zone} = \sum_{i=1}^{n_{soil}} f_{root_i} \times \frac{Wc_i - Wwilt_i}{Wfc_i - Wwilt_i} \quad (1)$$

185 where  $n_{soil}$  is the total number of soil layers in the root zone. This value depends on the considered vegetation type. For example,  $n_{soil} = 9$  for crops, with a rooting depth of 1.5 m.

In addition to sprinkler irrigation, the new model is able to represent drip or flood irrigation. In this case, the water flux is applied directly to the soil surface, with no leaf interception. Considering the static equipment used for drip irrigation, there is no irrigation interval ( $\Delta t_{\text{wn}} = 0$  day). In this study, only sprinkling irrigation is considered as this is the dominant irrigation type in Nebraska. Drip and flood irrigation will be evaluated in future works. The activation of a given irrigation method is described in Supplement S5. Irrigation simulations are illustrated in Supplements S2 and S3 over southwestern France and over the Hampton irrigated area in Nebraska (Fig. 1e and Figs. S1.2 and S1.3), respectively. Observed monthly precipitation in Nebraska is presented for contrasting years in Supplement S4.

All the values of the model parameters in Table 1 have been set within a default configuration. These values can be user-defined for each nature type and for each grid cell, including, when possible, seasonal variations. See Supplement S5 for configuration details and possibilities.

### **2.2.2 New aggregation rules of irrigated and rainfed vegetation**

The new crop and irrigation scheme is operated using ECOCLIMAP-SG (see Supplement S1). The best achievable spatial resolution of ECOCLIMAP-SG is  $300 \text{ m} \times 300 \text{ m}$ . In contrast to previous versions of ISBA, there is no specific irrigated nature type in the new ECOCLIMAP-SG vegetation description. On the other hand, irrigation of all the nature types listed in Table S1.2 is possible. By default, six vegetation types are considered (three crop and three woody vegetation types as shown in Fig. S1.1). The new crop and irrigation scheme is able to represent the sub-grid heterogeneity of the irrigation fractional coverage. This is illustrated over North America by Figs. S1.2 and S1.3, showing the fraction of irrigated C4 and C3 crops, respectively. For each nature type, an irrigated and a non-irrigated fraction are considered at the simulation resolution. In order to prevent an excessive increase in the number of simulated nature types (potentially 20 non-irrigated and 20 irrigated times 3 irrigation types, i.e. a total of 120 types), involving a large increase of complexity, memory and computing cost, some choices are made for the implementation:

1. Selection of a limited number of irrigated nature types. The default implementation consists in six irrigated nature types. Temperate deciduous and evergreen trees types (No 8 and 10 in Table S1.2, respectively) can be used to represent fruits trees or olive trees for example,

respectively. Shrub type (No 15) can be used to represent, among others, vine plants, and types No 19, 20 and 21 may represent irrigated crops (e.g. wheat, soybean, and corn, respectively).

2. Selection of the main irrigation method used for each grid cell and nature type, considering that in one grid cell there is only one dominant method for a given nature type (e.g. flooded rice in China or sprinkled corn in France).

Finally, the system state variables (soil water content, surface and soil temperature, vegetation biomass, etc.) differ in irrigated and non-irrigated parts of the cell. This implies to (1) duplicate a nature type if it is partially irrigated, (2) attribute for each grid cell the corresponding irrigated fraction, and (3) select the irrigation type for the irrigated fraction. Lastly, the two irrigated and non-irrigated nature types are treated separately but the same rooting depth and secondary parameters (see Table S1.1) are used.

In order to limit the computing time, vegetation types can (optionally) be gathered. In this case vegetation “patches” are created. In ISBA, patch aggregation (Masson et al., 2013) is a method used to reduce the number of simulated nature types. It is based on the aggregation of the fractions of nature types, as shown in Fig. 3. The model primary parameters such as rooting depth, LAI and tree height are weighted using the fractional coverage of each nature type in the grid cell. The mean parameter values are calculated following different laws: dominant, arithmetic averaging, inverse averaging or inverse of square logarithm averaging, depending on the considered parameters, as described in Noilhan and Lacarrère (1995) and Noilhan et al. (1997). In practice, the nature types to be aggregated (see the list in Fig. S1.1) within a grid cell are first chosen. Then, during the simulation, the fractions of nature type composing each patch are added together (step 1 in Fig. 3) for each grid cell. The different primary parameters (trees height, LAI, ...) are weighted by patch following the respective vegetation fractions (step 2 in Fig. 3). For secondary parameters (e.g. photosynthesis parameters in this study) a minimum number of patches is needed in order to avoid combining incompatible vegetation types (e.g. C3 crops and C4 crops).

240 In a first step (step 0 in Fig. 3) the differentiation between irrigated and rainfed nature types is done by computing the irrigated (and rainfed) fraction for each nature type and for each grid cell. Arithmetic averaging is used to cross information from the nature type fractional coverage and from the global irrigation fraction map described in Section 2.4.1. The ECOCLIMAP-SG land cover classification uses this additional data layer to compute the fraction of irrigated vegetation at the spatial  
245 resolution of the model simulations. Nature types considered as irrigated (by default 6) are duplicated (meaning that for each of them a new nature type is created with the same parameters). This ensures the distinction of irrigated and rainfed soil water budget types. Then, as before, the nature types are aggregated by patch and the primary parameter values are computed (step 1 and step 2 in Fig. 3, respectively).

250 This change of the code structure based on the aggregation tool is a way to (1) maintain the continuity with previous versions of the code, (2) ensure flexibility for the number of irrigated nature types to be considered and (3) simulate distinct irrigated and rainfed fractions of a nature type.

The new irrigation module represents water demand for irrigation, only, and irrigation is not explicitly limited by the lack of water resources. This has consequences on water conservation. Water  
255 used for irrigation is usually withdrawn from aquifers, rivers or reservoirs. These compartments are not represented in ISBA but a new module dedicated to dam/reservoirs is currently under development.

## 2.3 Experimental design

The simulations and the evaluation of the new irrigation scheme are made over the state of Nebraska (United States of America, USA). This area presents a high density of irrigated fields (Fig. 1) and large  
260 freely available observational datasets for evaluation. In this area, most irrigated field consist of corn (Zhang et al., 2020). In particular, we focus on a region where the irrigation is prominent: the south of the state of Nebraska (100-97°W, 40.25-41.25°N, Fig. 1e). The objective of the model evaluation is to demonstrate that the model is able to reproduce irrigation activities and that the irrigation scheme improves vegetation modelling and the associated surface fluxes as compared to observations.

265 The ISBA LSM simulations are made at a spatial resolution of  $0.25^\circ \times 0.25^\circ$ , over a 40-year period from 1979 to 2018. The initial values of the soil moisture and soil temperature profiles are

derived from a 20-year spin-up simulation by repeating year 1979. The same initial conditions are used for all the simulations, with and without crop and irrigation modelling. To evaluate the impact of irrigation, these simulations are run using the ECOCLIMAP-SG land cover classification within  
 270 SURFEX (see Supplement 1). All nature types are grouped into 15 patches including three irrigated ones: shrubs (orchards), C3 crops (typically wheat and rice) and C4 crops (corn). This study focuses on the results of these last two nature types because there are hardly any irrigated orchards in Nebraska in the irrigation map described in Section 2.4.1. The dates of the irrigation season for corn are chosen in accordance with the literature (USDA and NASS, 2010) from May (emergence) to September (harvest),  
 275 with a random picking of the day within those specific months. Three types of simulations are performed (Table 2): “ISBA\_ref” without irrigation nor crop phenology (the benchmark), “ISBA\_pheno” with only crop phenology attributes (emergence and harvest dates) and the complete “ISBA\_pheno\_irr” simulation with irrigation and crop phenology attributes. For the intercomparison of the simulations we select areas where the irrigation fractional coverage is larger than 50 % as  
 280 determined from the irrigation map, in order to better assess the local effects of irrigation in offline simulations.

The reference ISBA\_ref LAI simulations are compared with those from ISBA\_pheno and ISBA\_pheno\_irr experiments, and with the  $0.01^\circ \times 0.01^\circ$  LAI satellite observations over areas in Nebraska where the vegetation is considered as C3 or C4 irrigated crops by ECOCLIMAP-SG. In  
 285 addition to LAI, other variables are considered: gross primary production, evapotranspiration and land surface temperature. In order to compare the time series simulations with observations, the Pearson correlation coefficient ( $r$ ) and the root-mean-square difference (RMSD) scores are used. For water and carbon fluxes, they are calculated using daily values.

$$r = \frac{\sum_{i=1}^N (y_i - \bar{y})(x_i - \bar{x})}{\sqrt{\sum_{i=1}^N (y_i - \bar{y})^2 \sum_{i=1}^N (x_i - \bar{x})^2}} \quad (2)$$

290 where  $y$  and  $x$  stand for observations and model simulations, respectively, and

$$\bar{y} = \frac{1}{N} \sum_{i=1}^N y_i, \quad \bar{x} = \frac{1}{N} \sum_{i=1}^N x_i \quad (3)$$

are observation and model simulation means, respectively.

$$RMSE = \sqrt{\frac{1}{N} \sum_{i=1}^N (y_i - x_i)^2} \quad (4).$$

*N* represents the number of observations interpolated or aggregated to the model grid. *N* is equal to the  
 295 number of model grid-cells used in the calculation of the scores.

## 2.4 Data

### 2.4.1 Irrigation map

One of the main challenges of this study is to obtain an upgraded map of irrigation at the global scale, to be consistent with the resolution (300 m × 300 m) of the European Space Agency - Climate Change  
 300 Initiative (ESA-CCI) land cover map used in ECOCLIMAP-SG. The 1 km × 1 km resolution global irrigation map proposed by Meier et al. (2018), based on a statistical approach and satellite data, is used. A reason to choose this product is that its development process is based (amongst other) on the ESA-CCI land cover product (v1.6.1), the same as the one used to develop the ECOCLIMAP-SG vegetation map (Supplement S1).

305 In order to transfer the Meier irrigation map (1 km × 1 km) to ECOCLIMAP-SG (300 m × 300 m), a spatial resampling of the Meier map is performed (<https://doi.org/10.5281/zenodo.6011618>). A simple majority rule is used by assigning to each 300 m × 300 m grid point of ECOCLIMAP-SG the irrigation status (irrigated or rainfed) of the main corresponding grid-cell of the Meier 1 km × 1 km map. An irrigation map at a spatial resolution of 300 m × 300 m is obtained, with a single vegetation  
 310 type attributed to each grid cell together with the irrigation status. The main limitation of this map is that there is no information on the type of irrigation. In this study, we consider that all irrigation is of “sprinkler” type as this is the most common irrigation type in the USA and in Nebraska (AQUASTAT and FAO, 2019), where the testbed area of this study is located. This entails that irrigation water is added to the precipitation forcing over the irrigated agricultural parcels.

### 315 2.4.2 Atmospheric forcing

The simulations presented in this study are not coupled with the atmosphere. They are forced by a simulated atmospheric dataset of the European Centre for Medium-Range Weather Forecasts

(ECMWF): the ERA-5 atmospheric reanalysis at  $0.25^{\circ} \times 0.25^{\circ}$  (Hersbach et al., 2020). This global dataset was successfully used to force the ISBA LSM in previous studies (e.g. Albergel et al., 2019, 320 Bonan et al., 2020). Beck et al. (2019) show that the ERA-5 precipitation dataset is reasonably consistent with gauge-radar data over CONUS, except for mountainous areas. A subset of the ERA-5 forcing over Nebraska is used for the time period from 1979 to 2018. This period is chosen in order to encompass various validation datasets. The following atmospheric variables are used to force the ISBA LSM and are taken from ERA-5 at an hourly time step: air temperature, wind speed, air specific 325 humidity, atmospheric pressure, shortwave and longwave downwelling radiation and precipitation (liquid and solid).

### 2.4.3 Validation datasets

Six observation datasets are used (Table 3) to evaluate the simulations over Nebraska: the water used for irrigation, satellite-derived Leaf Area Index (LAI), gross primary production (GPP), 330 evapotranspiration, land surface temperature (LST), and precipitation.

Precipitation data from the Grand Island and Lincoln weather stations ( $40.93^{\circ}\text{N} - 98.76^{\circ}\text{W}$ ,  $40.83^{\circ}\text{N} - 96.76^{\circ}\text{W}$ , “Gi” dot in Fig. 1e and “Li” dot in Fig. 1b, respectively) are used to evaluate the ERA5 precipitation forcing over Nebraska. The two weather stations are within 170 km of each other and correspond to contrasting environmental conditions. While the Grand Island station is located 335 within a densely irrigated area, the Lincoln station is located at the Lincoln airport, which is surrounded by rainfed agricultural fields.

The water use records are provided by the US Geological Survey (USGS) through the National Water Information System (available at <https://waterdata.usgs.gov/ne/nwis/wu>, last access February 2022). Every 5 years from 1985 onward, the annual raw amount of water collected for irrigation is 340 available by county together with conveyance loss and with the surface area of the irrigated vegetation. This allows us to compute the amount of water used for irrigation per unit surface area (in mm) over the specific studied zone in Nebraska (Fig. 1e). The USGS data we use cover the 1985-2019 time period. Because conveyance loss data are not available for 1995, this year is not taken into account. In order to assess the consistency of the simulated irrigation process with observations, the simulated number of

345 yearly irrigation events on irrigated areas in Nebraska is compared with the USGS irrigation water  
amount estimates. Irrigation water amount is obtained from the simulated number of irrigation events  
using the model default irrigation water amount of 30 mm per irrigation event. Only values of the mean  
and standard deviation of the yearly irrigation amount are compared. The comparison is made for the  
irrigated croplands (either C3 or C4 crops) as defined using the irrigation map (Section 2.4.1) within the  
350 studied irrigated area in Nebraska (Fig. 1e).

The simulated LAI is compared with a satellite-derived LAI product at  $0.01^\circ \times 0.01^\circ$  spatial  
resolution derived from SPOT-VGT and PROBA-V satellite data (up to May 2014, and after May 2014,  
respectively) by the European Copernicus Global Land Service (CGLS). This LAI product is described  
in Baret et al. (2013). We use Version 2 of this product (GEOV2). It is available every 10 days from  
355 1999 onward. It does not cover the whole simulation time period (1979 to 2018).

The simulated GPP is compared to an upscaled estimate of GPP available at  $0.5^\circ$  from 1980 to  
2013, from the FLUXCOM project (Jung et al., 2017). Al-Yaari et al. (2021) show that the FLUXCOM  
daily evapotranspiration product can be used as a benchmark over irrigated areas. Since  
evapotranspiration and GPP fluxes are closely connected to each other, it can be assumed that the  
360 FLUXCOM GPP product is also sensitive to irrigation. The FLUXCOM product is based on a global  
machine learning model that does not have to be locally trained. However, it seems that three flux  
stations in Nebraska are used in the training as their data are included in the La Thuile dataset used to  
build FLUXCOM (Tramontana et al. 2016). These stations are located at 45 km at the north-east of the  
Lincoln weather station (e.g. Suyker and Verma, 2009), in a region where irrigation is present but not  
365 dominant.

The simulated evapotranspiration is compared to the GLEAM satellite-driven model estimates  
of land evapotranspiration available from 2003 to 2018 (version v3.2b, Martens et al., 2017). The  
GLEAM data come at the same  $0.25^\circ \times 0.25^\circ$  model's grid.

The simulated LST at 12h00 (local solar time) is compared to the LST derived from  
370 geostationary meteorological satellites by CGLS at 12h00 (local solar time). This product has a spatial  
resolution of  $0.05^\circ \times 0.05^\circ$  and is available from 2009 to 2018 (Freitas et al., 2013). It must be noticed

that in the version of the model used in this study, a single composite soil-vegetation energy budget is used and the thermal effect of crop residues is not represented. This means that over croplands, the simulated LST can differ from the vegetation temperature as seen from space.

375 In addition to the validation datasets, corn LAI observations at the field scale for various agricultural management conditions are available in Boedhram et al. (2001).

### 3 Results

The results presented below are focused on the impacts of the crop phenology and irrigation implementation on the simulated land surface variables over Nebraska. In addition to these results, 380 illustrations of the response to irrigation of simulated key land surface variables (SWI, LAI, GPP, evapotranspiration, LST) are shown over southwestern France and over the Hampton area in Nebraska in Supplements S2 and S3, respectively. In the case of Hampton, it can be noticed that the simulated irrigation mainly occurs in July and August (Fig. S3.1).

#### 3.1 Irrigation: water use

385 In Fig. 4, the mean yearly irrigation amount for C3 and C4 crops for the ISBA\_pheno\_irr experiment is compared to the values derived from the observations from the USGS. The simulated irrigation amount presents a large interannual variability, with a minimum of 60 mm in 1993 and a maximum close to 390 mm in 2002. It must be noticed that 1993 is one of the wettest year recorded at the Lincoln weather station (<https://lincolnweather.unl.edu/records/annual.asp>, last access May 2022). The mean 390 simulated value of the yearly irrigation water amount used for irrigation ( $271 \pm 75$  mm year<sup>-1</sup>) slightly overestimates the observed one ( $264 \pm 65$  mm year<sup>-1</sup>), with a difference of +2.7%. This difference could be explained by the availability of the water resource, not explicitly accounted for by the model yet. The large observed irrigation amounts in 2000 and 2005, larger than 300 mm year<sup>-1</sup>, are relatively well represented by the model. On the other hand, the observed small irrigation amount for the 2010 wet 395 year, is overestimated by about 110 mm year<sup>-1</sup>.

### 3.2 Irrigation: plant growth

Figure 5 illustrates the mean seasonal and interannual variability of LAI in the most densely irrigated part of Nebraska for areas with a fraction of irrigated crops larger than 50 % in Fig. 1e, from 1999 to 2018. Table 4 presents the peak LAI characteristics. While the satellite LAI observations present a peak  
400 at the end of July, the modelled LAI is plateauing in August (Fig. 5). The data from Boedhram et al. (2001) show that the modelled LAI plateau in August at LAI values of about  $3.5 \text{ m}^2 \text{ m}^{-2}$  is realistic for irrigated corn. The satellite LAI observations are sensitive to both rainfed and irrigated vegetation. In all ISBA LAI simulations, the start of the growing season corresponds to a gradual increase in LAI from the initial value of  $\text{LAI} = 0.30 \text{ m}^2 \text{ m}^{-2}$  imposed to the model in winter. The observed LAI presents a  
405 smaller minimum LAI value of  $0.15 \text{ m}^2 \text{ m}^{-2}$ , starts increasing in April and a value of  $0.30 \text{ m}^2 \text{ m}^{-2}$  is reached at the end of April. Then, plant growth continues at about the same low rate till the end of May. The LAI growth rate increases in June and LAI reaches a mean peak value of  $4.9 (\pm 0.8) \text{ m}^2 \text{ m}^{-2}$  is observed on 31 July (Table 4). The observed LAI then sharply decreases to reach its minimum value at about the end of September.

410 The ISBA\_ref LAI simulations do not mirror the observed late growing season and rapid senescence. The ISBA\_ref vs. observations comparison shows that without irrigation the simulated LAI generally starts increasing in March. On average, a peak LAI value of  $3.6 (\pm 0.2) \text{ m}^2 \text{ m}^{-2}$  is simulated by ISBA\_ref on 2 July, before slowly decreasing until the end of December. The ISBA\_ref growing season is much longer than observed. It starts two months before the observations and stops three months after  
415 the observations. The simulated LAI peaks one month before the observations. The simulated yearly LAI amplitude is 28 % smaller than observed.

The ISBA\_pheno LAI simulation is much more consistent with the LAI observations. The growing season starts in mid-May and the senescence ends at the end of September. However, the simulated peak LAI is still 30 % smaller than observed ( $\text{LAI} = 3.5 (\pm 0.2) \text{ m}^2 \text{ m}^{-2}$ ). The peak LAI is  
420 reached on 26 August, much later than the ISBA\_ref peak LAI, and about one month after the observed peak. The sharp decrease of LAI in September results from harvests at random dates in September. Adding irrigation (ISBA\_pheno\_irr) does not change the general pattern of the LAI curve, but increases

the LAI amplitude, with a mean peak LAI value of  $3.7 (\pm 0.1) \text{ m}^2 \text{ m}^{-2}$  on 28 August, larger (+8%) than for ISBA\_pheno but still below the observation (-24%).

425 The interannual variability of simulated and observed LAI values is illustrated in Fig. 5b, from 2002 to 2008. The ISBA\_ref LAI presents a systematic drop in summer, which is not present in the observations nor simulated by the ISBA\_pheno and ISBA\_pheno\_irr experiments. Without the regular seasonality imposed by crop phenology parameters, the model may simulate a re-growth of vegetation in autumn (e.g. in 2003), that is not present in the observations. The ISBA\_pheno and ISBA\_pheno\_irr  
430 simulations are more consistent with the observed seasonality.

### 3.3 Impact of crop phenology and irrigation on LAI at a regional scale

This section is focused on the impact of irrigation practices for the south Nebraska zone (as defined in Fig. 1e), and all nature types are considered for the comparison with observations at a spatial resolution of  $0.25^\circ \times 0.25^\circ$ .

435 Figure 6a shows the seasonal mean LAI variations from 1999 to 2018. This Figure is similar to Fig. 5a but all nature types are considered. Peak LAI characteristics are given in Table 4. They differ from the crop LAI peaks. While, the observed LAI peaks at  $3.8 (\pm 1.5) \text{ m}^2 \text{ m}^{-2}$  on 31 July for ISBA\_ref, LAI peaks at  $3.3 (\pm 0.3) \text{ m}^2 \text{ m}^{-2}$  on 1 July for ISBA\_ref,  $3.1 (\pm 0.3) \text{ m}^2 \text{ m}^{-2}$  on 16 July for ISBA\_pheno, and  $3.1 (\pm 0.3) \text{ m}^2 \text{ m}^{-2}$  on 16 July for ISBA\_pheno\_irr. Compared to crop simulations, the experiments  
440 with crop phenology (ISBA\_pheno and ISBA\_pheno\_irr) present earlier peak LAI dates, because rainfed vegetation affects the phenology. However, the irrigated crop signature is visible in the second peak of the annual LAI cycle simulated by ISBA\_pheno and ISBA\_pheno\_irr experiments at the end of August. More often than not (83 % and 88 % of the grid cells for  $r$  and RMSD, respectively) the LAI score differences between ISBA\_pheno\_irr and ISBA\_ref shown in Fig. 6 correspond to an  
445 improvement of the LAI simulation with the representation of irrigation. A month by month analysis of the scores (Fig. 7) shows a marked improvement of  $r$  values in June, July and September. The  $r$  value can frequently be increased by 30%. Lower RMSD values are observed from April to November, more frequently in May and in October. In April, October and November, the main cause of the reduction in RMSD values is the imposed minimum value of  $0.3 \text{ m}^2 \text{ m}^{-2}$  before the emergence (in May) and the

450 harvest (in September). The ISBA\_pheno correlation and RMSD differences with respect to ISBA\_ref are nearly identical to those showed for ISBA\_pheno\_irr in Figs. 6-7 (not shown).

### 3.4 Impact on the GPP flux

As the vegetation productivity is linked to LAI, the seasonality pattern of GPP (Fig. 8) is comparable to the one of LAI (Fig. 6) but the observed GPP peak ( $9.2 \pm 2.1 \text{ g[C]}\cdot\text{m}^{-2}\cdot\text{day}^{-1}$ ) occurs on mid-July while  
455 the observed LAI peaks on 31 July. During the plant growth period, the smallest differences between all the simulations and the observations occur at about the same time as the observed GPP peak. For all simulations, a GPP plateau at a value of  $9.0 \pm 1.8 \text{ g[C] m}^{-2} \text{ day}^{-1}$  is reached at the beginning of July and lasts until mid-July. Finally, the simulated GPP decreases in September with a delay of about two weeks with respect to the observations.

460 Before July, the ISBA\_ref photosynthetic activity is well in advance as compared to the observations, of about 20 days in May. This is consistent with the very large LAI values simulated by ISBA\_ref in May: about  $2 \text{ m}^2 \text{ m}^{-2}$ , while the mean LAI observation hardly exceeds  $0.5 \text{ m}^2 \text{ m}^{-2}$ . The simulated GPP maximum ( $9.7 \pm 2.0 \text{ g[C] m}^{-2} \text{ day}^{-1}$ ) is reached before the end of June. After a sharp decrease at the end of June, the ISBA\_ref GPP decreases at a slower rate than the observations. From  
465 mid-September to the end of October, the simulated GPP is much larger than the observed GPP.

The ISBA\_ref flaws are much less pronounced in ISBA\_pheno and ISBA\_pheno\_irr experiments. In the latter simulations, the increase of the GPP occurs at about the same time as in the observations. The GPP values are systematically larger with irrigation in July and August than for other simulations. As for LAI, the GPP  $r$  and RMSD scores (Fig. 8b and 8c, respectively) are better for  
470 ISBA\_pheno\_irr than for ISBA\_ref, with an improvement on 87 % and 81 % over the domain, respectively.

### 3.5 Impact on evapotranspiration

Investigating evapotranspiration is a way to assess the impact of irrigation on the hydrological system. Figure 9 shows evapotranspiration for the ISBA simulations and for GLEAM. This Figure is similar to  
475 Figs. 6 and 8 but a shorter time period is considered, from 2003 to 2018. Before the irrigation period,

the observed evapotranspiration steadily increases from February to July. After the irrigation period, evapotranspiration decreases until November. It can be observed that the short term variability of the GLEAM evapotranspiration is represented well by the simulations. On the other hand, all ISBA simulations produce much larger evapotranspiration values than GLEAM during the growing period  
 480 from April to June. For example, all ISBA simulations can reach  $5 \text{ mm day}^{-1}$  while GLEAM does not exceed  $3.5 \text{ mm day}^{-1}$ . Over this time period, ISBA\_ref overestimates evapotranspiration with respect to GLEAM by  $0.98 \pm 0.42 \text{ mm day}^{-1}$  ( $38 \pm 16 \%$ ) on average.

On the contrary, from mid-July to mid-August, all ISBA simulations tend to underestimate evapotranspiration with respect to GLEAM, by up to  $1.3 \text{ mm day}^{-1}$  for ISBA\_ref. Accounting for crop  
 485 phenology and irrigation into the model has a substantial impact on this variable and reduces the bias. Over the whole irrigation period, the mean bias goes from  $-0.4 \pm 0.4 \text{ mm day}^{-1}$  ( $-13 \pm 12 \%$ ) for ISBA\_ref to  $-0.2 \pm 0.3 \text{ mm day}^{-1}$  ( $-7 \pm 11 \%$ ) and  $-0.1 \pm 0.3 \text{ mm day}^{-1}$  ( $-2 \pm 11 \%$ ) for ISBA\_pheno and ISBA\_pheno\_irr, respectively. Evapotranspiration is overestimated again after the harvest, from mid-September to November by  $0.38 \pm 0.18 \text{ mm day}^{-1}$  ( $42 \pm 20 \%$  compared to the observations).

The newly implemented processes have a small but positive impact on the bias before and after the irrigation period. During the growing season, from April to June, the overestimation decreases from 38 % in ISBA\_ref to 33 % and 34 % for ISBA\_pheno and ISBA\_pheno\_irr, respectively. From mid-September to November, the overestimation decreases from 42 % to 35 % and 36 %, respectively. The  $r$  and RMSD differences between ISBA\_ref and ISBA\_pheno\_irr (Fig. 9) also show a global  
 495 improvement with 83 % and 79 % of the grid cells being improved. However, the effect on the  $r$  score is small (less than 0.1) and heterogeneous in time and space. Figure 10 shows that the  $r$  score is mainly improved in August and in September, before the harvest. Degradation in  $r$  can be observed at some locations throughout the growing season. The improvement of RMSD is more stable, and can be observed from May to October, the impact being more pronounced in July and August.

### 500 3.6 Impact on LST

In order to evaluate the impact of irrigation on the land surface energy budget, Fig. 11 shows land surface temperature at 12h00 local time simulated by the three model configurations and derived from

the CGLS product. Overall, ISBA tends to overestimate LST at noon, especially in April-May, up to 7 °C in Fig. 11a. The bias is reduced during the summer.

505 Due to the difficulty of observing the differences between the simulations, Fig. 11b presents differences of ISBA\_pheno and ISBA\_pheno\_irr versus ISBA\_ref. With crop phenology (with or without irrigation) the simulated LST is globally higher from April to June and from mid-September to November. The maximum difference with respect to ISBA\_ref is  $+0.7 \pm 0.3$  °C. It is observed for ISBA\_pheno in September. During the summer (July and August) the new model versions tend to  
510 present lower LST values, with temperature differences close to  $-0.2 \pm 0.1$  °C in ISBA\_pheno\_irr. Moreover, from May to mid-September the temperature in ISBA\_pheno\_irr is lower than in ISBA\_pheno, and this difference can reach locally -0.9°C in summer. Figure 12 presents the monthly *r* and RMSD scores of ISBA\_ref with respect to CGLS LST observations and the ISBA\_pheno\_irr score difference is shown. It shows that there is a seasonal dependence of these statistical values, with slightly  
515 better *r* and RMSD scores observed for ISBA\_pheno\_irr in July and August during the irrigation period. However, the representation of irrigation tends to degrade RMSD before (April, May) and after (October, November) the irrigation period.

## 4 Discussion and perspectives

The results presented in Section 3 show that the new version of ISBA is able to produce a realistic  
520 yearly irrigation water amount (Fig. 4). It also markedly improves the LAI and GPP simulations (Figs. 5-6 and Fig. 8, respectively). On the other hand, the new ISBA version developed in this study has a limited impact on the evapotranspiration and on the LST simulations and is not able to significantly reduce the strong model biases that are observed for these variables before and after the irrigation time period (Figs. 9-11).

### 525 4.1 Could the new crop and irrigation scheme be further improved?

The crop phenology model is very simple and adding more parameters related to phenology could be a way to further improve the model performance. Integrating satellite LAI observations in ISBA using

sequential data assimilation is also an option (Mucia et al., 2020). The results of our numerical experiments over Nebraska show that considering crop phenology improves the consistency of the simulations with LAI and GPP observations. The corresponding correlation and RMSD scores are improved. The crop phenology parameters used to force emergence and harvest dates reduce the length of the growing season, delay spring growth and avoid a regrowth in the autumn. It seems that irrigation only plays an additive role in improving the vegetation seasonal cycle as compared to the role of including crop phenology (Section 3.3). Both crop phenology and irrigation models have shortcomings and their performance could be limited by difficulties in simulating processes that are not directly related to irrigation.

Firstly, the same emergence and harvest dates are imposed for all years, while in reality crop phenology may present an inter-annual variability related to climate conditions. This is particularly the case for Nebraska because the start of the growing season depends on the snowmelt and soil thawing dates. These processes are represented in ISBA and crop phenology parameters could be related to snow melting and soil thawing, but this would require extensive developments to be implemented at a global scale. Moreover, the representation of the cold season processes is not perfect in ISBA (Decharme et al. 2019) and the model tends to underestimate snow depth and the length of the snow season. This could explain biases in soil temperature and LST simulations before and after the irrigation time period. Figure 11 shows that LST values below the freezing level can be observed in April and that their model counterparts are about 7 °C warmer. The earlier thawing in model simulations is reflected in the much earlier leaf onset in LAI simulations. Figure 6 shows that while the observed LAI does not exceed 0.5 m<sup>2</sup> m<sup>-2</sup> at the end of April, the ISBA\_ref LAI reaches the same value about one month earlier. The unrealistically early leaf onset is consistent with the warm model bias at the end of the cold season. This shows that improving the representation of the cold season by assimilating satellite-derived or in situ snow cover fraction observations could improve the simulation of the crop growing period in this area. Also, emergence and harvest dates could be derived from the LAI observation in order to better represent the interannual variation. However, the currently used empirical approach to establish the crop season provides robust results over the irrigated grid cells (Fig. 5).

555 Secondly, the irrigation itself is based on fixed parameter values such as the minimum period  
between two consecutive irrigations (one week) and SWI levels triggering irrigation turns. The  
simulations over the Hampton grid cell show that the first irrigation can start at quite low levels of the  
SWI (Fig. S3.1), even below the second irrigation threshold of 0.55 defined in Section 2.2.1.  
Suppressing the one week constraint of irrigation turns improves the simulation of the peak LAI, which  
560 otherwise is rather poorly simulated (Fig. 5). However, this change triggers unrealistic large irrigation  
water amounts (not shown). A lack of irrigation water amount cannot explain the excessive soil water  
deficit. One could also challenge the quality of the ERA5 precipitation. Figure S4.1 and Fig. S4.2 show  
that ERA5 precipitation compares well with in situ observations and that the seasonal and inter-annual  
variability is fairly represented. A more plausible explanation could be that the initial soil water storage  
565 value between the end of the cold season and the first irrigation turn is withdrawn too quickly from the  
soil by the model. This explanation would be consistent with the marked overestimation of  
evapotranspiration in spring, from April to June (Fig. 9), before the irrigation time period.

A possible limitation of using a global low-resolution reanalysis such as ERA5 is that changes to  
the local climatic conditions caused by irrigation may not be represented. Over Nebraska, Szilagyi and  
570 Franz (2020) show that the decadal increase in irrigated land tends to trigger a reduction in precipitation  
over the most densely irrigated areas, of about -10 mm per decade. The largest precipitation suppression  
is observed at Spring, in March, before the corn growing season, in relation to larger soil water content  
values. In our simulations, ISBA\_pheno\_irr presents larger soil moisture values than ISBA\_ref in March  
(see Fig. S3.1), but this is mainly due to crop phenology. The ERA5 screen-level 2 m air temperature  
575 and relative humidity are analyzed together with soil moisture by assimilating in situ observations from  
ground weather stations (Hersbach et al. 2020). In large irrigated areas where weather stations are  
present, the assimilation should be able to represent the soil moisture effect on these variables, even at  
coarse spatial resolution. A large-scale experiment involving ground and airborne measurements was  
recently performed in northeastern Spain to assess the impact of irrigation on atmospheric model  
580 simulations (Boone et al. 2021).

## 4.2 Are evaporation components simulated well?

In order to investigate the evapotranspiration bias in Spring, the evaporation components are plotted in Fig. S3.3 and Fig. S3.4 for the Hampton irrigated area in 2018. Figure S3.3 shows that total evapotranspiration of ISBA\_ref and ISBA\_pheno\_irr are quite similar. This is consistent with the small impact of crop phenology on total evapotranspiration showed in Fig. 9. On the other hand, soil evaporation and plant transpiration differ. In the ISBA\_pheno\_irr simulation, transpiration is reduced in Spring by more than 30 %, in comparison with ISBA\_ref. The lower transpiration is offset by larger soil evaporation values. As a result, total evapotranspiration does not change much and the bias is not reduced in ISBA\_pheno\_irr. Also, Fig. S3.4 shows that the new crop and irrigation module does not affect interception much. Therefore, the ISBA\_pheno\_irr evapotranspiration bias in spring could be caused by the large soil evaporation. The evaporation component could be overestimated because (1) the soil is too warm in relation to a poor representation of thawing or because (2) crop residues at the soil surface are not represented. Wortmann et al. (2012) show that in this area, not harvesting crop residues tends to reduce soil evaporation and increase crop yield, limit water runoff, soil erosion, and contributes to maintaining soil fertility. Suyker and Verma (2009) show that increasing surface mulch dry mass from 50 to 150 g m<sup>-2</sup> can decrease the non-growing season evapotranspiration by more than 20 %. The ISBA model includes a representation of litter in forests (Napoly et al. 2017) that will be generalized to low vegetation in the next version of SURFEX. Using this new capability could improve our simulations.

Finally, degradation in  $r$  for evapotranspiration in Fig. 10 may be evidence that GLEAM may not be considered as a suitable reference for evapotranspiration comparisons in areas impacted by irrigation. The use of other datasets is investigated in Supplement 3. In particular, in situ observations over an irrigated corn field (Suyker and Verma, 2009) are used. Table S3.1 shows that GLEAM tends to underestimate evapotranspiration by 20 % during the growing season (from May to September). During the non-growing season, the ISBA\_pheno\_irr model overestimates evapotranspiration by 48 %. Table S3.2 and Fig. S3.5 show that the ISBA\_pheno\_irr evapotranspiration peak (in June) tends to happen too early. Mean values of near-surface wind speed are particularly large over Nebraska, especially at

wintertime and springtime (Chen, 2020). This feature could exacerbate the impact of a misrepresentation of soil evaporation.

610

### **4.3 Is the irrigation scheme flexible enough?**

In this study, sprinkling irrigation is considered. The model is able to represent other irrigation systems such as flooding irrigation but more developments are needed to limit the runoff to the irrigated plot and this options needs to be validated. The newly implemented irrigation processes, along with the new  
615 ECOCLIMAP-SG vegetation description let users choose which nature type should be irrigated. Irrigation can be represented at various spatial scales, ranging from the field scale for agricultural studies to the global scale for climate studies. Model parameters can be specified using new datasets or local characteristics. For example, in this article we use a unique date for starting and ending the crop growing season with a random variability, but more accurate dates can be prescribed (varying spatially  
620 and from one vegetation type to another, or using crop calendars). Moreover, the better spatial resolution of ECOCLIMAP-SG allows the use of high resolution atmospheric forcing. This provides new opportunities for assessing the impact of irrigation on local climate and water resource conditions.

This study is mainly focused on a zone in the south of Nebraska where the irrigation density is relatively high (Fig. 1), and results could differ in other regions. Except for the fixed emergence and  
625 harvesting dates corresponding to regional crop phenology (from USDA and NASS, 2010), default values are used for all the other parameters (Section 2.4). Tests performed in southwestern France (Supplement S2) allow ensuring that the model is able to work in contrasting climate conditions.

In this study, the ISBA simulations are not coupled to the atmosphere, nor to the CTRIP river routing system. Such coupled numerical experiments can be performed thanks to the SURFEX  
630 modelling platform. However, more developments are needed in order to ensure water conservation in the hydrological system. In particular, irrigation water amounts should be consistent with the available water resource in rivers, groundwater, and dams.

## 5 Conclusions

A new uncalibrated irrigation scheme is implemented within the ISBA land surface model in order to improve the representation of vegetation over agricultural areas. A case study over an irrigated area in the state of Nebraska (USA) is performed to validate the new scheme. Simple crop phenology rules represent emergence and harvesting and improve the seasonality of plant growth, while the additional water supply from the irrigation mostly impacts the peak LAI value. The model is able to produce a realistic yearly irrigation water amount and markedly improves the LAI and GPP. It is shown that model performance can be limited by processes not directly related to irrigation, such as thawing or crop residues. The irrigation scheme has many possible configurations and the code is highly flexible. With this capability, ancillary data on farming practices such as emergence and harvest dates, or the amount of water per irrigation event, can be used. This flexible crop phenology and irrigation scheme can take the spatial heterogeneity of irrigation activities into account, and detect irrigation-induced impacts on Earth system simulations. Our results show that crop phenology parameters modify the seasonal pattern of the simulation of LAI, soil moisture, evapotranspiration and plant carbon uptake, and that irrigation affects their magnitude. This provides the basis for further development in offline and online applications of the ISBA model.

### Code availability

The ISBA land surface model is available as open source via the SURFEX modelling platform, available at <https://www.umr-cnrm.fr/surfex/spip.php?article387>. It is under a CECILL-C License (French equivalent to the L-GPL licence). The version developed and use for the experiment in this study is available on: <https://doi.org/10.5281/zenodo.5718063>. It based on the SURFEX version 8.1 (ref f70f6457). For future use, it is strongly recommended to use the newest version of ISBA, from the version 9.0 (scheduled for release in 2022) from which the irrigation developed will be included by default. Initialization files are available on: <https://doi.org/10.5281/zenodo.6011618>.

## **Author contribution**

Arsène Druel and Clément Albergel designed the experiments. Arsène Druel carried out the  
660 implementation of the irrigation scheme and performed the simulations. Arsène Druel wrote the  
manuscript. All co-authors participated to the analysis of the results and to the revision of the  
manuscript.

## **Competing interests**

The authors declare that they have no conflicts of interest.

## **665 Acknowledgments**

The work presented here was supported by the project URCLIM (advance on URban CLIMate services,  
part of ERA4CS, an ERA-NET initialised by JPI Climate with co-funding of the European Union  
(Grant n°690462)). The authors would like to thanks Stephanie Faroux and Marie Minvielle in charge  
of the SURFEX code support for technical assistance, and Deborah Verfaillie for her careful reading of  
670 the manuscript.

## References

- Adegoke, J. O., Pielke, R. A., Eastman, J., Mahmood, R. and Hubbard, K. G.: Impact of Irrigation on Midsummer Surface Fluxes and Temperature under Dry Synoptic Conditions: A Regional Atmospheric Model Study of the U.S. High Plains, *Mon. Weather Rev.*, 131(3), 556–564, [https://doi.org/10.1175/1520-0493\(2003\)131<0556:IOIOMS>2.0.CO;2](https://doi.org/10.1175/1520-0493(2003)131<0556:IOIOMS>2.0.CO;2), 2003.
- Al-Yaari, A., A. Ducharne, S. Tafasca, H. Mizuochi and F. Cheruy, "Influence of irrigation on the bias between ORCHIDEE and FLUXCOM evapotranspiration products," 2021 IEEE International Geoscience and Remote Sensing Symposium IGARSS, 6552-6555, <https://doi.org/10.1109/IGARSS47720.2021.9554734>, 2021.
- AQUASTAT and FAO: Country Fact Sheet, United States of America, [online] Available from: [http://www.fao.org/nr/water/aquastat/data/cf/readPdf.html?f=USA-CF\\_eng.pdf](http://www.fao.org/nr/water/aquastat/data/cf/readPdf.html?f=USA-CF_eng.pdf) (Accessed 20 March 2019), 2019.
- Baret, F., Weiss, M., Lacaze, R., Camacho, F., Makhmara, H., Pacholczyk, P. and Smets, B.: GEOV1: LAI and FAPAR essential climate variables and FCOVER global time series capitalizing over existing products. Part1: Principles of development and production, *Remote Sens. Environ.*, 137, 299–309, <https://doi.org/10.1016/j.rse.2012.12.027>, 2013.
- Beck, H. E., Pan, M., Roy, T., Weedon, G. P., Pappenberger, F., van Dijk, A. I. J. M., Huffman, G. J., Adler, R. F., and Wood, E. F.: Daily evaluation of 26 precipitation datasets using Stage-IV gauge-radar data for the CONUS, *Hydrol. Earth Syst. Sci.*, 23, 207–224, <https://doi.org/10.5194/hess-23-207-2019>, 2019.
- Biemans, H., Haddeland, I., Kabat, P., Ludwig, F., Hutjes, R. W. A., Heinke, J., von Bloh, W. and Gerten, D.: Impact of reservoirs on river discharge and irrigation water supply during the 20th century, *Water Resour. Res.*, 47(3), <https://doi.org/10.1029/2009WR008929>, 2011.
- Boedhram, N., T. J. Arkebauer, and W. D. Batchelor: Season-long characterization of vertical distribution of leaf area in corn, *Agron. J.*, 93, 1235–1242, <https://doi.org/10.2134/agronj2001.1235>, 2001.
- Bonnemort, C., Bouthier, A., Deumier, J.-M., and Specty, R.: Conduire l'irrigation avec Irritel ; intérêts

- et limites, *La Météorologie*, 14, 36-43, <https://doi.org/10.4267/2042/51182>, 1996.
- 700 Boone, A., J. Bellvert, M. Best, J. Brooke, G. Canut-Rocafort, J. Cuxart, O. Hartogensis, P. Le Moigne, J. R. Miró, J. Polcher, J. Price, P. Quintana Seguí, M. Wooster, 2021: Updates on the international Land Surface Interactions with the Atmosphere over the Iberian Semi-Arid Environment (LIAISE) Field Campaign. *GEWEX News*, 31(4), 16-21, available on [https://www.gewex.org/gewex-content/files\\_mf/1640101560Q42021.pdf](https://www.gewex.org/gewex-content/files_mf/1640101560Q42021.pdf), last access February 2022, 2021.
- 705 Broadbent, A. M., Coutts, A. M., Tapper, N. J. and Demuzere, M.: The cooling effect of irrigation on urban microclimate during heatwave conditions, *Urban Clim.*, 23, 309–329, <https://doi.org/10.1016/j.uclim.2017.05.002>, 2018.
- Brown, T. C., Foti, R. and Ramirez, J. A.: Projected freshwater withdrawals in the United States under a changing climate, *Water Resour. Res.*, 49(3), 1259–1276, <https://doi.org/10.1002/wrcr.20076>, 2013.
- 710 Bruinsma, J.: The Resource Outlook to 2050: By How Much Do Land, Water Use and Crop Yields Need to Increase by 2050?, Food and Agriculture Organization, Rome, Italy., 2009.
- Calvet, J.-C., and Champeaux J.-L.: L’apport de la télédétection spatiale à la modélisation des surfaces continentales. *La Météorologie*, 108, 52-58, <https://doi.org/10.37053/lameteorologie-2020-0016>, 2020.
- 715 Calvet, J.-C., Gibelin, A.-L., Roujean, J.-L., Martin, E., Le Moigne, P., Douville, H. and Noilhan, J.: Past and future scenarios of the effect of carbon dioxide on plant growth and transpiration for three vegetation types of southwestern France, *Atmospheric Chem. Phys.*, 8(2), 397–406, <https://doi.org/10.5194/acp-8-397-2008>, 2008.
- Calvet, J.-C., Noilhan, J., Roujean, J.-L., Bessemoulin, P., Cabelguenne, M., Olioso, A. and Wigneron, J.-P.: An interactive vegetation SVAT model tested against data from six contrasting sites, *Agric. For. Meteorol.*, 92(2), 73–95, [https://doi.org/10.1016/S0168-1923\(98\)00091-4](https://doi.org/10.1016/S0168-1923(98)00091-4), 1998.
- 720 Carrillo-Guerrero, Y., Glenn, E. P. and Hinojosa-Huerta, O.: Water budget for agricultural and aquatic ecosystems in the delta of the Colorado River, Mexico: Implications for obtaining water for the environment, *Ecol. Eng.*, 59, 41–51, <https://doi.org/10.1016/j.ecoleng.2013.04.047>, 2013.
- 725 Chen, L.: Impacts of climate change on wind resources over North America based on NA-CORDEX,

- Renewable Energy, 153, 1428-1438, <https://doi.org/10.1016/j.renene.2020.02.090>, 2020.
- Chukalla, A. D., Krol, M. S. and Hoekstra, A. Y.: Green and blue water footprint reduction in irrigated agriculture: effect of irrigation techniques, irrigation strategies and mulching, *Hydrol. Earth Syst. Sci.*, 19(12), 4877–4891, <https://doi.org/10.5194/hess-19-4877-2015>, 2015.
- 730 Colaizzi, P. D., Gowda, P. H., Marek, T. H. and Porter, D. O.: Irrigation in the Texas High Plains: a brief history and potential reductions in demand, *Irrig. Drain.*, 58(3), 257–274, <https://doi.org/10.1002/ird.418>, 2009.
- DeAngelis, A., Dominguez, F., Fan, Y., Robock, A., Kustu, M. D. and Robinson, D.: Evidence of enhanced precipitation due to irrigation over the Great Plains of the United States, *J. Geophys. Res.*, 735 115(D15), D15115, <https://doi.org/10.1029/2010JD013892>, 2010.
- Decharme, B., Delire, C., Minvielle, M., Colin, J., Vergnes, J., Alias, A., Saint-Martin, D., Sférian, R., Sénési, S. and Voldoire, A.: Recent Changes in the ISBA-CTRIP Land Surface System for Use in the CNRM-CM6 Climate Model and in Global Off-Line Hydrological Applications, *J. Adv. Model. Earth Syst.*, 11(5), 1207–1252, <https://doi.org/10.1029/2018MS001545>, 2019.
- 740 de Vrese, P., Hagemann, S. and Claussen, M.: Asian irrigation, African rain: Remote impacts of irrigation, *Geophys. Res. Lett.*, 43, 3737-3745, <https://doi.org/10.1002/2016GL068146>, 2016.
- Döll, P., Fiedler, K. and Zhang, J.: Global-scale analysis of river flow alterations due to water withdrawals and reservoirs, *Hydrol. Earth Syst. Sci.*, 13(12), 2413–2432, <https://doi.org/10.5194/hess-13-2413-2009>, 2009.
- 745 Döll, P., Hoffmann-Dobrev, H., Portmann, F. T., Siebert, S., Eicker, A., Rodell, M., Strassberg, G. and Scanlon, B. R.: Impact of water withdrawals from groundwater and surface water on continental water storage variations, *J. Geodyn.*, 59–60, 143–156, <https://doi.org/10.1016/j.jog.2011.05.001>, 2012.
- Douglas, E. M., Niyogi, D., Frolking, S., Yeluripati, J. B., Pielke, R. A., Niyogi, N., Vörösmarty, C. J. 750 and Mohanty, U. C.: Changes in moisture and energy fluxes due to agricultural land use and irrigation in the Indian Monsoon Belt, *Geophys. Res. Lett.*, 33(14), L14403, <https://doi.org/10.1029/2006GL026550>, 2006.

- Evans, R. G. and Sadler, E. J.: Methods and technologies to improve efficiency of water use, *Water Resour. Res.*, 44(7), <https://doi.org/10.1029/2007WR006200>, 2008.
- 755 FAO: Food and Agriculture Organization of the United Nations: Water withdrawal and pressure on water resources, [online] Available from: <http://www.fao.org/nr/water/aquastat/didyouknow/index2.stm>, [http://www.fao.org/nr/water/aquastat/infographics/Withdrawal\\_eng.pdf](http://www.fao.org/nr/water/aquastat/infographics/Withdrawal_eng.pdf) (Accessed 9 October 2019), 2014.
- 760 Faroux, S., Kaptué Tchuenté, A. T., Roujean, J.-L., Masson, V., Martin, E. and Le Moigne, P.: ECOCLIMAP-II/Europe: a twofold database of ecosystems and surface parameters at 1 km resolution based on satellite information for use in land surface, meteorological and climate models, *Geosci. Model Dev.*, 6(2), 563–582, <https://doi.org/10.5194/gmd-6-563-2013>, 2013.
- Felfelani, F., D. M. Lawrence, and Y. Pokhrel: Representing intercell lateral groundwater flow and  
765 aquifer pumping in the community land model, *Water Resources Research*, 56, e2020WR027531, <https://doi.org/10.1029/2020WR027531>, 2020.
- Field, C. B., Barros, V. R., Dokken, D. J., Mach, K. J. and Mastrandrea, M. D., Eds.: *Climate Change 2014 Impacts, Adaptation, and Vulnerability: Working Group II Contribution to the Fifth Assessment Report of the Intergovernmental Panel on Climate Change*, Cambridge University Press,  
770 Cambridge., 2014.
- Fischer, C., Montmerle, T., Berre, L., Auger, L. and Ștefănescu, S. E.: An overview of the variational assimilation in the ALADIN/France numerical weather-prediction system, *Q. J. R. Meteorol. Soc.*, 131(613), 3477–3492, <https://doi.org/10.1256/qj.05.115>, 2005.
- Fraiture, C. de, Wichelns, D., Rockström, J., Kemp-Benedict, E., Eriyagama, N., Gordon, L. J., Hanjra, M. A., Hoogeveen, J., Huber-Lee, A. and Karlberg, L.: Looking ahead to 2050: scenarios of  
775 alternative investment approaches, in In Molden, David (Ed.). *Water for food, water for life: a Comprehensive Assessment of Water Management in Agriculture.*, pp. 91–145, International Water Management Institute (IWMI), London, UK: Earthscan; Colombo, Sri Lanka. [online] Available from: <https://hdl.handle.net/10568/36869>, 2007.

- 780 Freitas, S. C., Trigo, I. F., Macedo, J., Barroso, C., Silva, R. and Perdigão, R.: Land surface temperature from multiple geostationary satellites, *Int. J. Remote Sens.*, 34(9–10), 3051–3068, <https://doi.org/10.1080/01431161.2012.716925>, 2013.
- Gibelin, A.-L., Calvet, J.-C., Roujean, J.-L., Jarlan, L. and Los, S. O.: Ability of the land surface model ISBA-A-gs to simulate leaf area index at the global scale: Comparison with satellites products, *J. Geophys. Res.*, 111(D18), D18102, <https://doi.org/10.1029/2005JD006691>, 2006.
- 785 Grafton, R. Q., Williams, J., Perry, C. J., Molle, F., Ringler, C., Steduto, P., Udall, B., Wheeler, S. A., Wang, Y., Garrick, D. and Allen, R. G.: The paradox of irrigation efficiency, *Science*, 361(6404), 748–750, <https://doi.org/10.1126/science.aat9314>, 2018.
- Haddeland, I., Skaugen, T. and Lettenmaier, D. P.: Anthropogenic impacts on continental surface water fluxes, *Geophys. Res. Lett.*, 33(8), L08406, <https://doi.org/10.1029/2006GL026047>, 2006.
- 790 Hanasaki, N., Inuzuka, T., Kanae, S. and Oki, T.: An estimation of global virtual water flow and sources of water withdrawal for major crops and livestock products using a global hydrological model, *J. Hydrol.*, 384(3–4), 232–244, <https://doi.org/10.1016/j.jhydrol.2009.09.028>, 2010.
- Harding, R. J., Blyth, E. M., Tuinenburg, O. A. and Wiltshire, A.: Land atmosphere feedbacks and their role in the water resources of the Ganges basin, *Sci. Total Environ.*, 468–469, S85–S92, <https://doi.org/10.1016/j.scitotenv.2013.03.016>, 2013.
- 795 Hersbach, H., Bell, B., Berrisford, P., Hirahara, S., Horányi, A., Muñoz-Sabater, J., Nicolas, J., Peubey, C., Radu, R., Schepers, D., Simmons, A., Soci, C., Abdalla, S., Abellan, X., Balsamo, G., Bechtold, P., Biavati, G., Bidlot, J., Bonavita, M., De Chiara, G., Dahlgren, P., Dee, D., Diamantakis, M., Dragani, R., Flemming, J., Forbes, R., Fuentes, M., Geer, A., Haimberger, L., Healy, S., Hogan, R. J., Hólm, E., Janisková, M., Keeley, S., Laloyaux, P., Lopez, P., Lupu, C., Radnoti, G., de Rosnay, P., Rozum, I., Vamborg, F., Villaume, S., and Thépaut, J.-N.: The ERA5 Global Reanalysis, *Q. J. Roy. Meteor. Soc.*, 146, 730, 1999–2049, <https://doi.org/10.1002/qj.3803>, 2020.
- 800 Hoekstra, A. Y. and Mekonnen, M. M.: The water footprint of humanity, *Proc. Natl. Acad. Sci.*, 109(9), 3232–3237, <https://doi.org/10.1073/pnas.1109936109>, 2012.
- Jägermeyr, J., Gerten, D., Heinke, J., Schaphoff, S., Kummu, M., and Lucht, W.: Water savings

- potentials of irrigation systems: global simulation of processes and linkages, *Hydrol. Earth Syst. Sci.*, 19, 3073–3091, <https://doi.org/10.5194/hess-19-3073-2015>, 2015.
- Jiang, L., Ma, E. and Deng, X.: Impacts of Irrigation on the Heat Fluxes and Near-Surface Temperature  
810 in an Inland Irrigation Area of Northern China, *Energies*, 7(3), 1300–1317, <https://doi.org/10.3390/en7031300>, 2014.
- Jung, M., Reichstein, M., Schwalm, C. R., Huntingford, C., Sitch, S., Ahlström, A., Arneth, A., Camps-Valls, G., Ciais, P., Friedlingstein, P., Gans, F., Ichii, K., Jain, A. K., Kato, E., Papale, D., Poulter, B., Raduly, B., Rödenbeck, C., Tramontana, G., Viovy, N., Wang, Y.-P., Weber, U., Zaehle, S. and  
815 Zeng, N.: Compensatory water effects link yearly global land CO<sub>2</sub> sink changes to temperature, *Nature*, 541(7638), 516–520, <https://doi.org/10.1038/nature20780>, 2017.
- Khan, S. and Abbas, A.: Upscaling water savings from farm to irrigation system level using GIS-based agro-hydrological modelling, *Irrig. Drain.*, 56(1), 29–42, <https://doi.org/10.1002/ird.284>, 2007.
- Koech, R. and Langat, P.: Improving Irrigation Water Use Efficiency: A Review of Advances,  
820 Challenges and Opportunities in the Australian Context, *Water*, 10(12), 1771, <https://doi.org/10.3390/w10121771>, 2018.
- Kueppers, L. M., Snyder, M. A. and Sloan, L. C.: Irrigation cooling effect: Regional climate forcing by land-use change, *Geophys. Res. Lett.*, 34(3), L03703, <https://doi.org/10.1029/2006GL028679>, 2007.
- Lawston, P. M., Santanello, J. A., Zaitchik, B. F. and Rodell, M.: Impact of Irrigation Methods on Land  
825 Surface Model Spinup and Initialization of WRF Forecasts, *J. Hydrometeorol.*, 16(3), 1135–1154, <https://doi.org/10.1175/JHM-D-14-0203.1>, 2015.
- Le Moigne, P. et al.: SURFEX scientific documentation - V8.1, Sci. Doc. - SURFEX [online] Available from: <http://www.umr-cnrm.fr/surfex/spip.php?rubrique11> (Accessed 26 February 2018), 2018.
- Lobell, D. B., Bonfils, C. J., Kueppers, L. M. and Snyder, M. A.: Irrigation cooling effect on  
830 temperature and heat index extremes, *Geophys. Res. Lett.*, 35(9), L09705, <https://doi.org/10.1029/2008GL034145>, 2008.
- Martens, B., Miralles, D. G., Lievens, H., van der Schalie, R., de Jeu, R. A. M., Fernández-Prieto, D., Beck, H. E., Dorigo, W. A. and Verhoest, N. E. C.: GLEAM v3: satellite-based land evaporation and

- 835 root-zone soil moisture, *Geosci. Model Dev.*, 10(5), 1903–1925, <https://doi.org/10.5194/gmd-10-1903-2017>, 2017.
- Masson, V., Le Moigne, P., Martin, E., Faroux, S., Alias, A., Alkama, R., Belamari, S., Barbu, A., Boone, A., Bouyssel, F., Brousseau, P., Brun, E., Calvet, J.-C., Carrer, D., Decharme, B., Delire, C., Donier, S., Essaouini, K., Gibelin, A.-L., Giordani, H., Habets, F., Jidane, M., Kerdraon, G., Kourzeneva, E., Lafaysse, M., Lafont, S., Lebeaupin Brossier, C., Lemonsu, A., Mahfouf, J.-F., 840 Marguinaud, P., Mokhtari, M., Morin, S., Pigeon, G., Salgado, R., Seity, Y., Taillefer, F., Tanguy, G., Tulet, P., Vincendon, B., Vionnet, V. and Voldoire, A.: The SURFEXv7.2 land and ocean surface platform for coupled or offline simulation of earth surface variables and fluxes, *Geosci. Model Dev.*, 6(4), 929–960, <https://doi.org/10.5194/gmd-6-929-2013>, 2013.
- Meier, J., Zabel, F. and Mauser, W.: A global approach to estimate irrigated areas &ndash; a 845 comparison between different data and statistics, *Hydrol. Earth Syst. Sci.*, 22(2), 1119–1133, <https://doi.org/10.5194/hess-22-1119-2018>, 2018.
- Mucia, A., Bonan, B., Zheng, Y., Albergel, C., and Calvet, J.-C.: From monitoring to forecasting land surface conditions using a land data assimilation system: Application over the contiguous United States, *Remote Sens.*, 12, <https://doi.org/10.3390/rs12122020>, 2020.
- 850 Munier, S. and Decharme, B.: River network and hydro-geomorphology parametrization for global river routing modelling at 1/12° resolution, *Earth Syst. Sci. Data Discuss.* [preprint], <https://doi.org/10.5194/essd-2021-434>, in review, 2021.
- Noilhan, J. and Lacarrère, P.: GCM Grid-Scale Evaporation from Mesoscale Modeling, *J. Clim.*, 8(2), 206–223, [https://doi.org/10.1175/1520-0442\(1995\)008<0206:GGSEFM>2.0.CO;2](https://doi.org/10.1175/1520-0442(1995)008<0206:GGSEFM>2.0.CO;2), 1995.
- 855 Noilhan, J. and Planton, S.: A Simple Parameterization of Land Surface Processes for Meteorological Models, *Mon. Weather Rev.*, 117(3), 536–549, [https://doi.org/10.1175/1520-0493\(1989\)117<0536:ASPOLS>2.0.CO;2](https://doi.org/10.1175/1520-0493(1989)117<0536:ASPOLS>2.0.CO;2), 1989.
- Noilhan, J., Lacarrère, P., Dolman, A. J. and Blyth, E. M.: Defining area-average parameters in meteorological models for land surfaces with mesoscale heterogeneity, *J. Hydrol.*, 190(3–4), 302– 860 316, [https://doi.org/10.1016/S0022-1694\(96\)03131-9](https://doi.org/10.1016/S0022-1694(96)03131-9), 1997.

- Ozdogan, M., Rodell, M., Beaudoin, H. K. and Toll, D. L.: Simulating the Effects of Irrigation over the United States in a Land Surface Model Based on Satellite-Derived Agricultural Data, *J. Hydrometeorol.*, 11(1), 171–184, <https://doi.org/10.1175/2009JHM1116.1>, 2010.
- Perry, C.: Efficient irrigation; Inefficient communication; Flawed recommendations, *Irrig. Drain.*, 56, 367–378, 2007.
- Perry, C., Steduto, P., Allen, R. G., and Burt, C. M.: Increasing productivity in irrigated agriculture: Agronomic constraints and hydrological realities, *Agr. Water Manage.*, 96, 1517–1524, 2009.
- Perry, C., Steduto, P. and Karejeh, F.: Does Improved Irrigation Technology Save Water? A Review of the Evidence, Food and Agriculture Organization, Cairo, Egypt, ISBN 978-92-5-109774-8, 2017.
- Pfeiffer, L. and Lin, C.-Y. C.: Does efficient irrigation technology lead to reduced groundwater extraction? Empirical evidence, *J. Environ. Econ. Manag.*, 67(2), 189–208, <https://doi.org/10.1016/j.jeem.2013.12.002>, 2014.
- Piao, S., Ciais, P., Huang, Y., Shen, Z., Peng, S., Li, J., Zhou, L., Liu, H., Ma, Y., Ding, Y., Friedlingstein, P., Liu, C., Tan, K., Yu, Y., Zhang, T. and Fang, J.: The impacts of climate change on water resources and agriculture in China, *Nature*, 467(7311), 43–51, <https://doi.org/10.1038/nature09364>, 2010.
- Puma, M. J. and Cook, B. I.: Effects of irrigation on global climate during the 20th century, *J. Geophys. Res.*, 115(D16), D16120, <https://doi.org/10.1029/2010JD014122>, 2010.
- Rodell, M., Velicogna, I. and Famiglietti, J. S.: Satellite-based estimates of groundwater depletion in India, *Nature*, 460(7258), 999–1002, <https://doi.org/10.1038/nature08238>, 2009.
- Rost, S., Gerten, D., Bondeau, A., Lucht, W., Rohwer, J. and Schaphoff, S.: Agricultural green and blue water consumption and its influence on the global water system: GLOBAL WATER USE IN AGRICULTURE, *Water Resour. Res.*, 44(9), <https://doi.org/10.1029/2007WR006331>, 2008.
- Sacks, W. J., Cook, B. I., Buening, N., Levis, S. and Helkowski, J. H.: Effects of global irrigation on the near-surface climate, *Clim. Dyn.*, 33(2–3), 159–175, <https://doi.org/10.1007/s00382-008-0445-z>, 2009.
- Saeed, F., Hagemann, S. and Jacob, D.: Impact of irrigation on the South Asian summer monsoon,

- Geophys. Res. Lett., 36(20), L20711, <https://doi.org/10.1029/2009GL040625>, 2009.
- Shukla, S. P., Puma, M. J. and Cook, B. I.: The response of the South Asian Summer Monsoon  
890 circulation to intensified irrigation in global climate model simulations, *Clim. Dyn.*, 42(1–2), 21–36,  
<https://doi.org/10.1007/s00382-013-1786-9>, 2014.
- Siebert, S. and Döll, P.: Quantifying blue and green virtual water contents in global crop production as  
well as potential production losses without irrigation, *J. Hydrol.*, 384(3–4), 198–217,  
<https://doi.org/10.1016/j.jhydrol.2009.07.031>, 2010.
- 895 Siebert, S., Kummu, M., Porkka, M., Döll, P., Ramankutty, N. and Scanlon, B. R.: A global data set of  
the extent of irrigated land from 1900 to 2005, *Hydrol. Earth Syst. Sci.*, 19(3), 1521–1545,  
<https://doi.org/10.5194/hess-19-1521-2015>, 2015.
- Sorooshian, S., Li, J., Hsu, K. and Gao, X.: Influence of irrigation schemes used in regional climate  
models on evapotranspiration estimation: Results and comparative studies from California’s Central  
900 Valley agricultural regions: INFLUENCE OF IRRIGATION IN RCM ON ET, *J. Geophys. Res.*  
*Atmospheres*, 117(D6), <https://doi.org/10.1029/2011JD016978>, 2012.
- Suyker, A. E. and Verma, S. B.: Evapotranspiration of irrigated and rainfed maize–soybean cropping  
systems, *Agric. For. Meteorol.*, 149, 443–452, <https://doi.org/10.1016/j.agrformet.2008.09.010>, 2009.
- Szilagyi, J., Franz, T.E.: Anthropogenic hydrometeorological changes at a regional scale: observed  
905 irrigation–precipitation feedback (1979–2015) in Nebraska, USA, *Sustain. Water Resour. Manag.* 6,  
10 pp., <https://doi.org/10.1007/s40899-020-00368-w>, 2020.
- Tang, Q., Oki, T., Kanae, S. and Hu, H.: Hydrological Cycles Change in the Yellow River Basin during  
the Last Half of the Twentieth Century, *J. Clim.*, 21(8), 1790–1806,  
<https://doi.org/10.1175/2007JCLI1854.1>, 2008.
- 910 Tramontana, G., Jung, M., Schwalm, C. R., Ichii, K., Camps-Valls, G., Ráduly, B., Reichstein, M.,  
Arain, M. A., Cescatti, A., Kiely, G., Merbold, L., Serrano-Ortiz, P., Sickert, S., Wolf, S., and  
Papale, D.: Predicting carbon dioxide and energy fluxes across global FLUXNET sites with  
regression algorithms, *Biogeosciences*, 13, 4291–4313, <https://doi.org/10.5194/bg-13-4291-2016>,  
2016.

- 915 United Nations, Department of Economic and Social Affairs and Population Division: World population prospects Data booklet, 2019 revision Data booklet, 2019 revision., 2019.
- USDA and NASS: Farm and ranch irrigation (2008), Special Studies in 2007 Census Publications, United States Department of Agriculture, National Agricultural Statistics Service, AC-07-SS-1. [online] Available from:
- 920 [https://www.nass.usda.gov/Publications/AgCensus/2007/Online\\_Highlights/Farm\\_and\\_Ranch\\_Irrigation\\_Survey/fris08.pdf](https://www.nass.usda.gov/Publications/AgCensus/2007/Online_Highlights/Farm_and_Ranch_Irrigation_Survey/fris08.pdf), 2009.
- USDA and NASS: Field Crops, Usual Planting and Harvesting Dates, United States Department of Agriculture - National Agricultural Statistics Service. [online] Available from: [https://downloads.usda.library.cornell.edu/usda-](https://downloads.usda.library.cornell.edu/usda-esmis/files/vm40xr56k/dv13zw65p/w9505297d/planting-10-29-2010.pdf)
- 925 [esmis/files/vm40xr56k/dv13zw65p/w9505297d/planting-10-29-2010.pdf](https://downloads.usda.library.cornell.edu/usda-esmis/files/vm40xr56k/dv13zw65p/w9505297d/planting-10-29-2010.pdf) (Accessed 4 July 2019), 2010.
- Verburg, P. H., Dearing, J. A., Dyke, J. G., Leeuw, S. van der, Seitzinger, S., Steffen, W. and Syvitski, J.: Methods and approaches to modelling the Anthropocene, *Glob. Environ. Change*, 39, 328–340, <https://doi.org/10.1016/j.gloenvcha.2015.08.007>, 2016.
- 930 Voirin-Morel, S.: Hydrographical modelling at a regional scale : application to the Adour-Garonne basin, Toulouse 3., 2003.
- Voldoire, A., Decharme, B., Pianezze, J., Lebeaupin Brossier, C., Sevault, F., Seyfried, L., Garnier, V., Bielli, S., Valcke, S., Alias, A., Accensi, M., Arduin, F., Bouin, M.-N., Ducrocq, V., Faroux, S., Giordani, H., Léger, F., Marsaleix, P., Rainaud, R., Redelsperger, J.-L., Richard, E. and Riette, S.: SURFEX v8.0 interface with OASIS3-MCT to couple atmosphere with hydrology, ocean, waves and sea-ice models, from coastal to global scales, *Geosci. Model Dev.*, 10(11), 4207–4227, <https://doi.org/10.5194/gmd-10-4207-2017>, 2017.
- 935 Zaitchik, B. F., Evans, J. and Smith, R. B.: MODIS-Derived Boundary Conditions for a Mesoscale Climate Model: Application to Irrigated Agriculture in the Euphrates Basin, *Mon. Weather Rev.*, 133(6), 1727–1743, <https://doi.org/10.1175/MWR2947.1>, 2005.
- 940 Zhang, G., D. Shen, B. Ming, R. Xie, X. Jin, C. Liu, P. Hou, J. Xue, J. Chen, W. Zhang, W. Liu, K.

Wang, S. Li: Using irrigation intervals to optimize water-use efficiency and maize yield in Xinjiang, northwest China, *The Crop J.*, 7, 322-334, <https://doi.org/10.1016/j.cj.2018.10.008>, 2019.

945 Zhang, Z., M. Barlage, F. Chen, Y. Li, W. Helgason, X. Xu, X. Liu, and Z. Li: Joint modeling of crop and irrigation in the central United States using the Noah-MP land surface model. *Journal of Advances in Modeling Earth Systems*, 12, e2020MS002159, <https://doi.org/10.1029/2020MS002159>, 2020.

950

**Table 1 – Irrigation parameters.**

Symbol	Definition	Default value (this study)
$I_T$	Irrigation type	sprinkler
$I_{NT}$	Irrigated nature type	C3 crops, C4 crops, shrubs
$I_W$	Water amount per irrigation water turn	30 mm
$I_D$	Irrigation water turn duration	8 hours
$SWI_1$	SWI threshold for triggering the first water turn	0.70
$SWI_2$	SWI threshold for triggering the second water turn	0.55
$SWI_3$	SWI threshold for triggering the third water turn	0.40
$SWI_{4+i}$	SWI threshold for triggering the following water turns (i, integer > 0)	0.25
$\Delta t_{Wn}$	Minimum time lapse between two water turns (irrigation interval)	7 days (0 days for drip irrigation)
$\Delta t_{WH}$	Minimum time lapse between the last water turn and the harvest	15 days
$t_E$	Emergence date	15 May ( $\pm$ 15 days)
$t_H$	Harvest date	15 September ( $\pm$ 15 days)

955

**Table 2 – Main set up of the three 40-year evaluation experiments forced by ERA-5 atmospheric variables over Nebraska. Crop phenology is defined by emergence and harvest dates, while irrigation corresponds to additional water supply.**

960

Experiment	Crop phenology	Irrigation	Forcing	Spinup time	Simulation time period
ISBA_ref	no	no	ERA-5 $0.25^\circ \times 0.25^\circ$	20 years	1979-2018
ISBA_pheno	YES	no			
ISBA_pheno_irr	YES	YES			

965

**Table 3 – Evaluation datasets.**

Observations	Source	Reference	Spatial resolution	Time period	Sampling time
Water used for irrigation	USGS	<a href="https://waterdata.usgs.gov/ne/nwis/wu">https://waterdata.usgs.gov/ne/nwis/wu</a>	County	1985-2015	5 years
LAI	CGLS	Baret et al., 2013	0.01°	1999-2018	10 days
GPP	FLUXCOM	Jung et al., 2017	0.25°	1980-2013	1 day
Evapotranspiration	GLEAM	Martens et al., 2017	0.25°	2003-2018	1 day
Land surface temperature at 12h	CGLS	Freitas et al., 2013	0.05°	2009-2018	1 day
In situ precipitation	University of Nebraska-Lincoln	<a href="http://climod.unl.edu/">http://climod.unl.edu/</a>	local	2009-2012	Monthly

970

**Table 4 – Observed and simulated mean LAI peak characteristics over Nebraska for the 1999-2018 time period for crops (see Fig. 5) and all vegetation types (see Fig. 6).**

Vegetation types	LAI source	Peak LAI (m <sup>2</sup> m <sup>-2</sup> )	Peak LAI date
Crops	Satellite observations	4.9 (±0.8)	31 July
	Boedhram et al. 2001 (*)	3.6 to 4.0	12 July to 19 August 1994
	Boedhram et al. 2001 (*)	3.5	2 August to 23 August 1995
	ISBA_ref	3.6 (±0.2)	2 July
	ISBA_pheno	3.5 (±0.2)	26 August
	ISBA_pheno_irr	3.7 (±0.1)	28 August
All	Satellite observations	3.8 (±1.5)	31 July
	ISBA_ref	3.3 (±0.3)	1 July
	ISBA_pheno	3.1 (±0.3)	16 July
	ISBA_pheno_irr	3.1 (±0.3)	16 July

(\*) Boedhram et al. (2001) data are for fertilized irrigated corn in 1994 and 1995

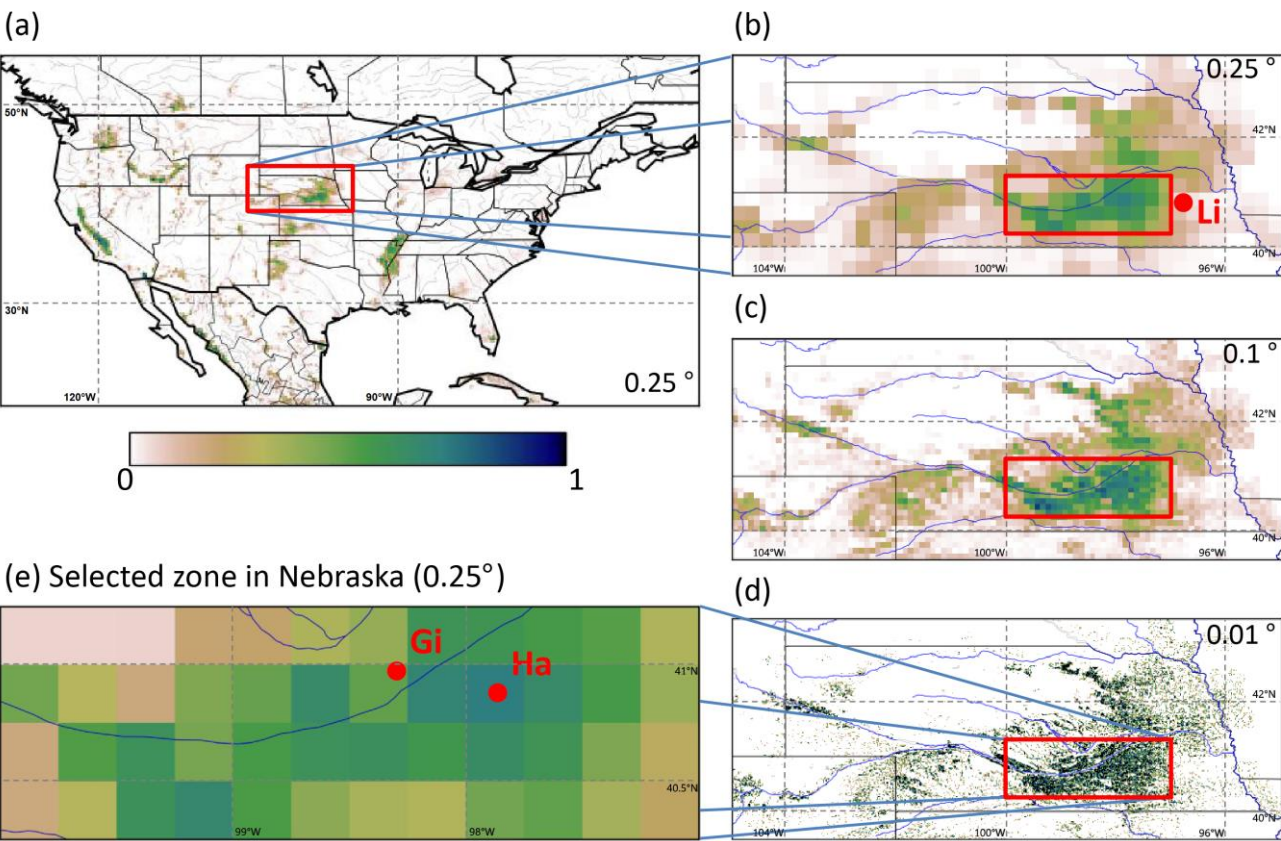


**Figure 1 – Irrigation fractional coverage derived from Meier et al. (2018) over (a) the Continental United State (CONUS), (b, c, d, e) Nebraska: at (b) 0.25°×0.25°, (c) 0.1°×0.1°, (d) 0.01°×0.01° spatial resolutions, and (e) over the selected zone in southern Nebraska considered in this study (100-97°W, 40.25-41.25°N). The red boxes show the location of the different zooms. The “Li”, “Gi” and “Ha” red dots correspond to the Lincoln weather station, Grand Island weather station, and Hampton irrigated area, respectively.**

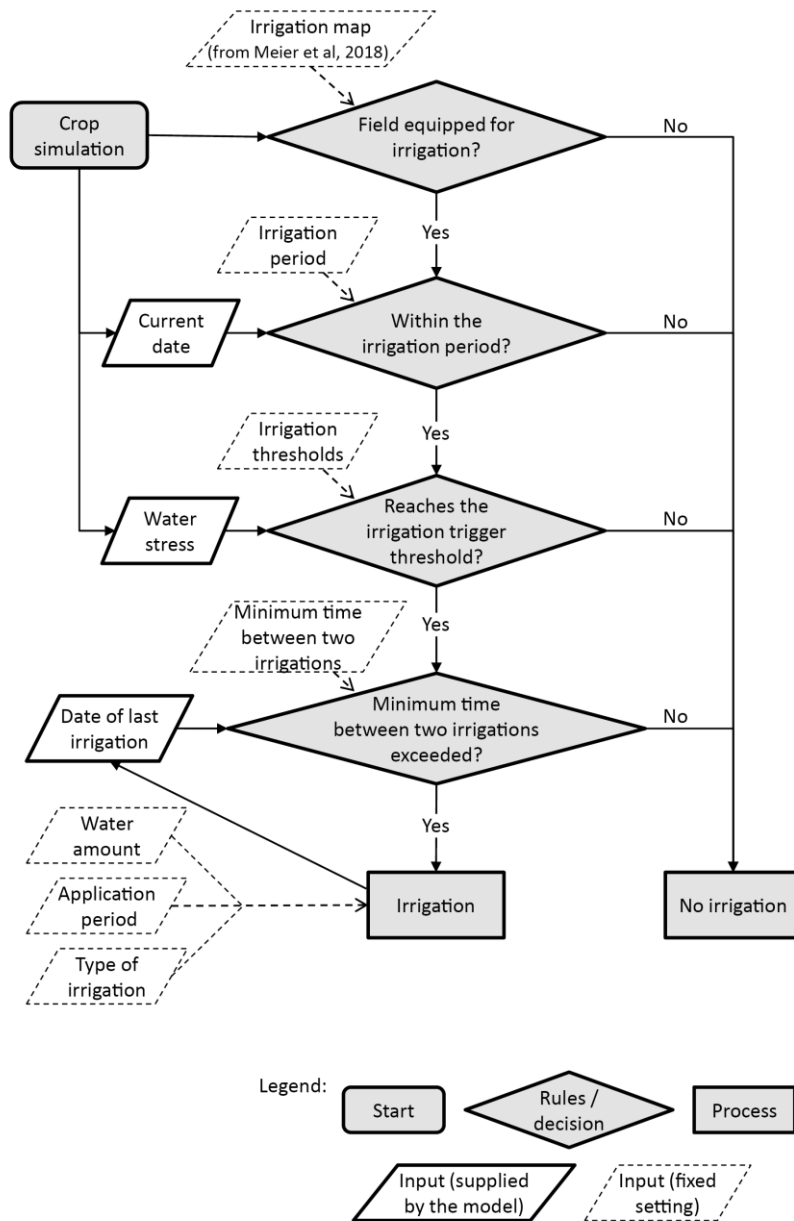
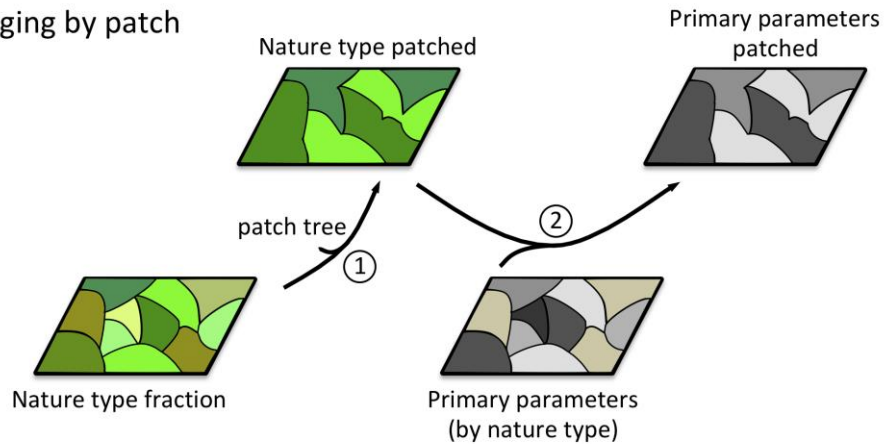


**Figure 2 – Irrigation decision tree model.**

(a) Standard nature type merging by patch



(b) Nature type distributed with irrigation and merging by patch

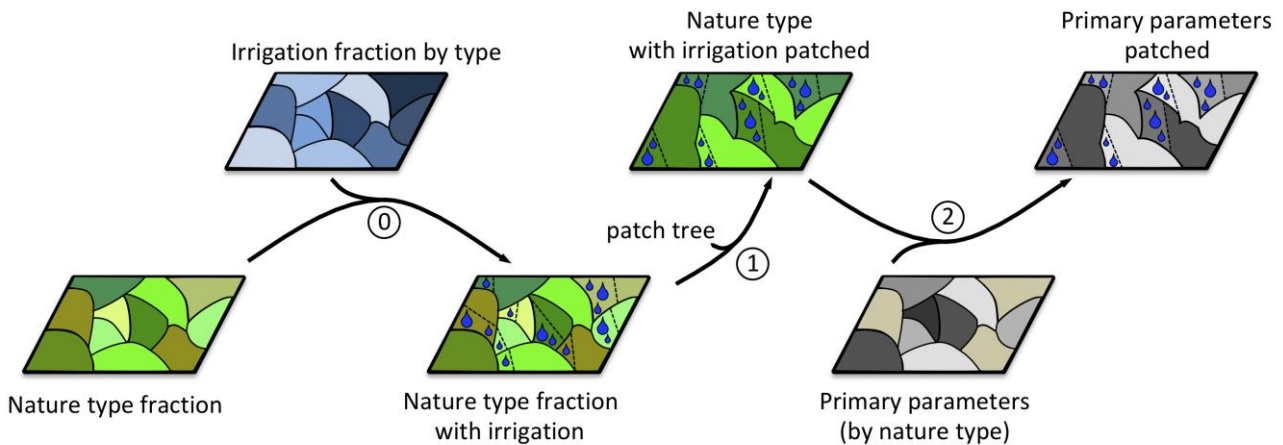
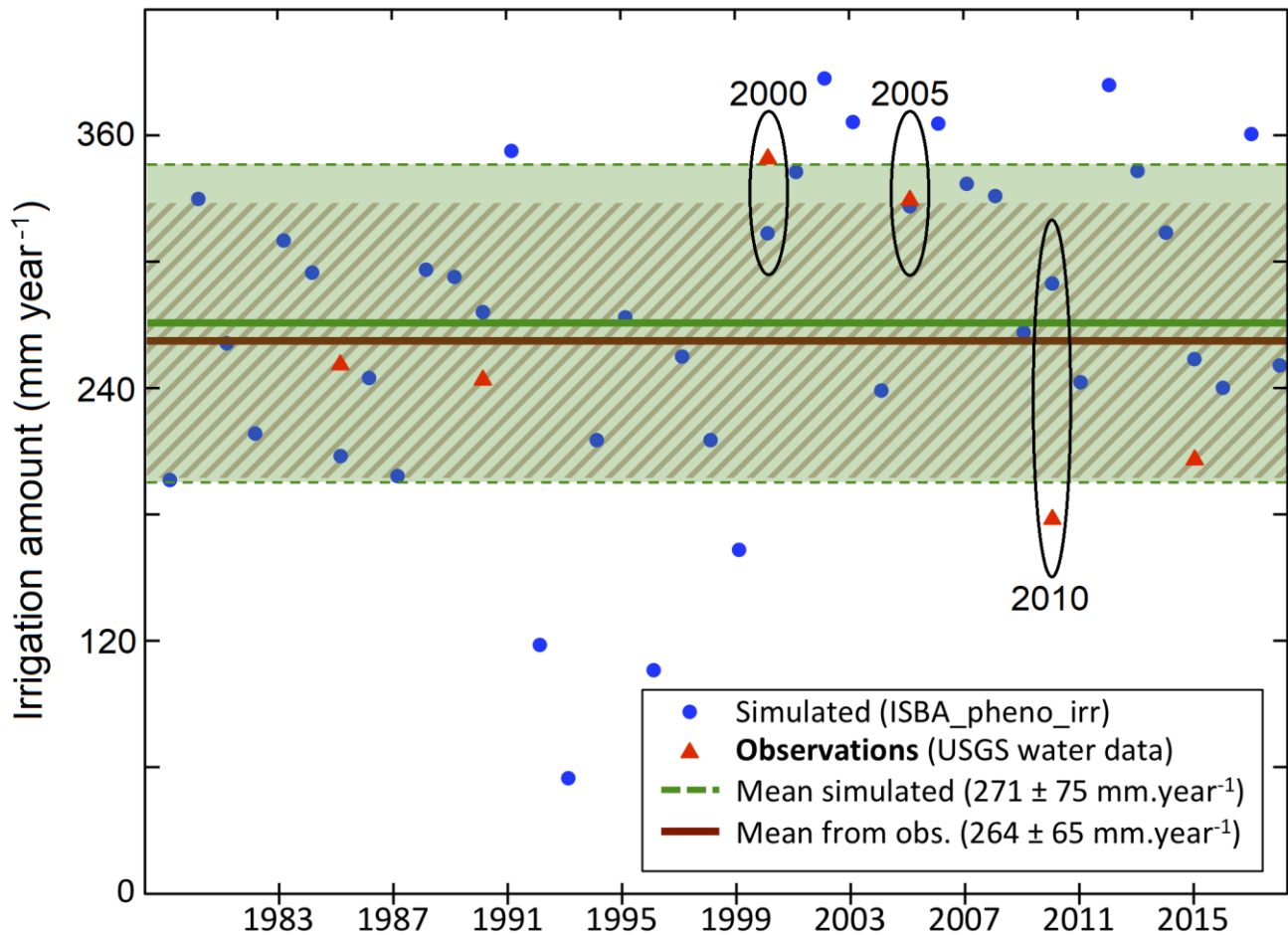


**Figure 3 – Diagram of the processing steps to obtain the ISBA model primary parameters from the nature types: (a) with the original method and (b) with the new method developed for irrigation. The different steps consist of: (0) cross-referencing the maps of vegetation cover (nature types) and irrigation fractional coverage (addition of irrigated nature type classes where irrigation is possible), (1) merging nature type classes following path aggregation rules (see Fig. S1.1), and (2) computing primary parameter values following the patch fraction map.**



1000 **Figure 4 – Yearly cumulated irrigation amounts simulated by the model for the studied area in Nebraska from 1979 to 2018 (blue line). The mean and standard deviation of the yearly values are shown for the model (green solid and dashed lines, respectively), and for the USGS water data from 1985 to 2019 (brown lines). The 2000 and 2005 dry years are indicated, together with the 2010 wet year.**

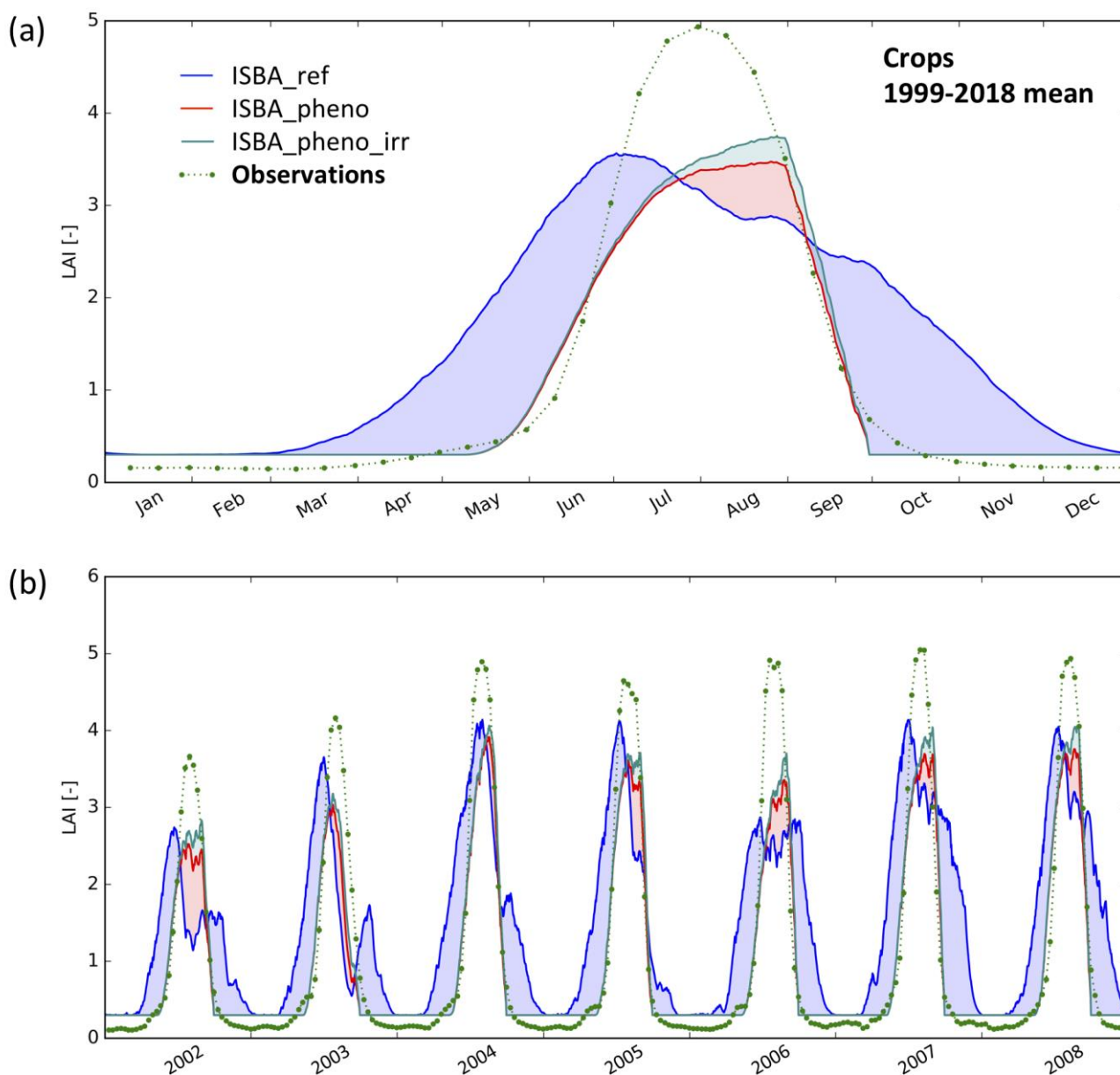


**Figure 5 – LAI ( $\text{m}^2 \text{ m}^{-2}$ ) of irrigated crops (C3 or C4) in the most densely irrigated part of Nebraska (Fig. 1e): (a) seasonal variation for the time period from 1999 to 2018, (b) daily time series from 2002 to 2008. Simulated LAI is shown for the irrigated fraction, from the reference simulation (ISBA\_ref, blue line), and from the simulations with only agricultural practices and with agricultural practices and irrigation (ISBA\_pheno, red line, and ISBA\_pheno\_irr, cyan line, respectively). Satellite-derived LAI observations (green dots) are for areas where the fraction of C3 or C4 irrigated crops is larger than 50 %.**

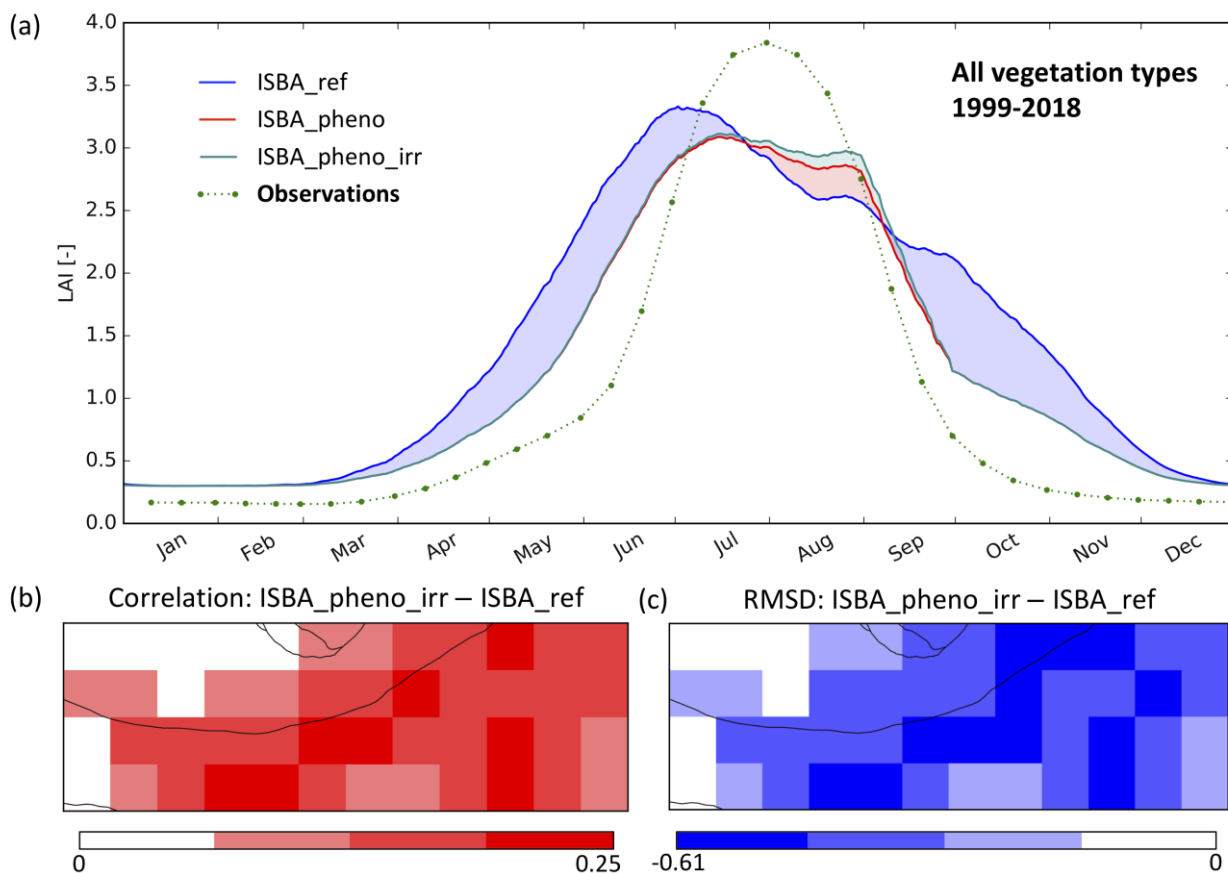


**Figure 6 – Simulated vs. observed LAI ( $\text{m}^2\text{m}^{-2}$ ) of all vegetation types, in the most densely irrigated part of Nebraska (Fig. 1e) from 1999 to 2018: (a) seasonal variation of mean LAI of ISBA\_ref (blue line), ISBA\_pheno (red line), ISBA\_pheno\_irr (cyan) simulations and of satellite-derived observations (green dots), (b) temporal correlation and (c) RMSD score difference maps showing the added value of the ISBA\_pheno\_irr with respect to ISBA-ref. Positive value for correlation (Fig. 6b) means that the result of ISBA\_pheno\_irr is better, and for RMSD (Fig. 6c) negative value means that result of ISBA\_pheno\_irr is better.**

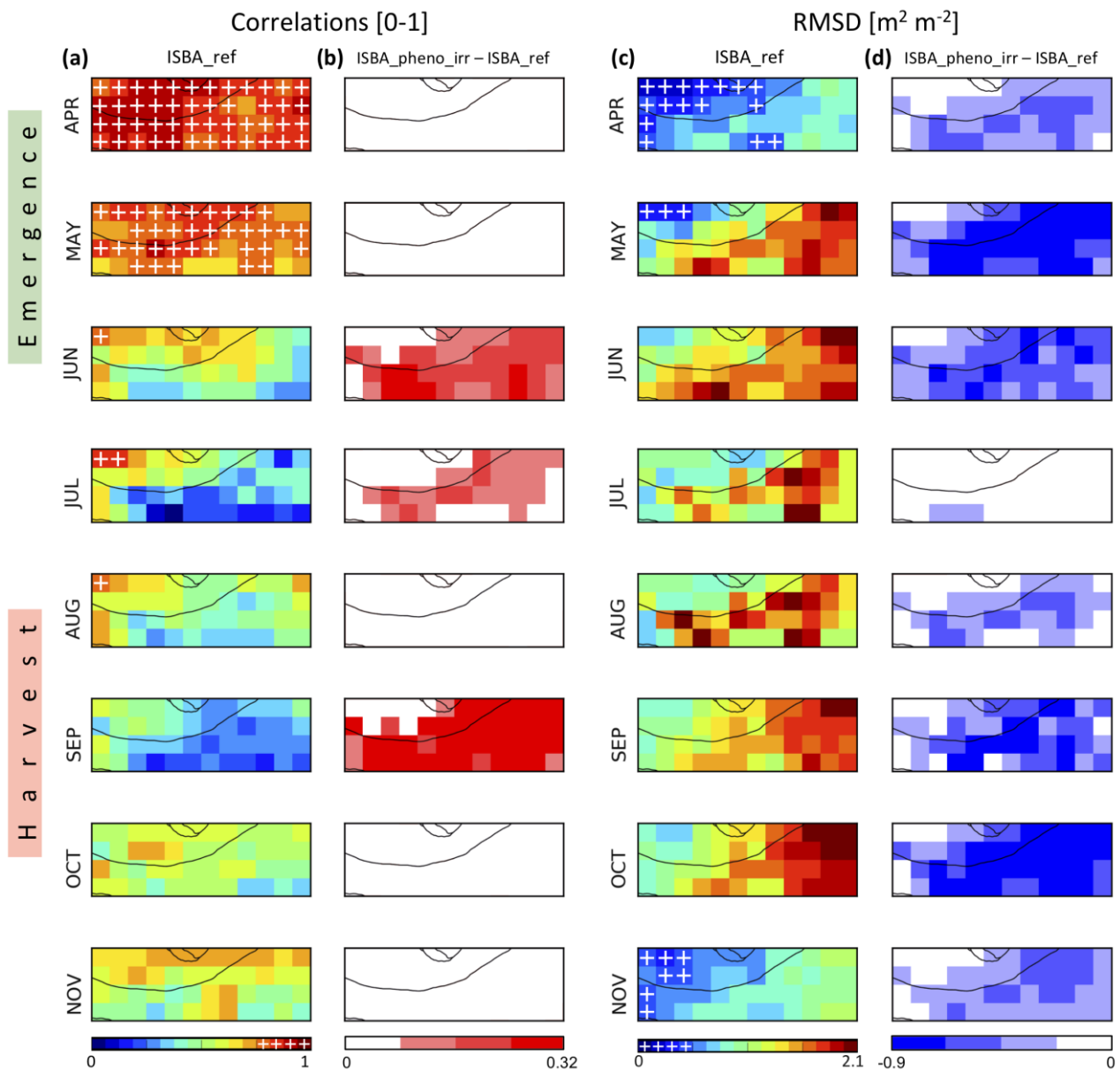


**Figure 7 – Comparison of simulated LAI with CGLS LAI observations in the most densely irrigated part of Nebraska (Fig. 1e) from 1999 to 2018 during the vegetation growing and senescence time period from April to November. Monthly temporal correlation (a, b) and RMSD (c, d) maps are shown for the reference simulation without a representation of irrigation ISBA\_ref (a, c). The added value of the ISBA\_pheno\_irr simulation with respect to ISBA-ref is shown through score difference maps (b, d). ISBA\_ref correlations (RMSD) values larger (smaller) than 0.75 (0.525 m² m⁻²) are indicated by white plus symbols.**

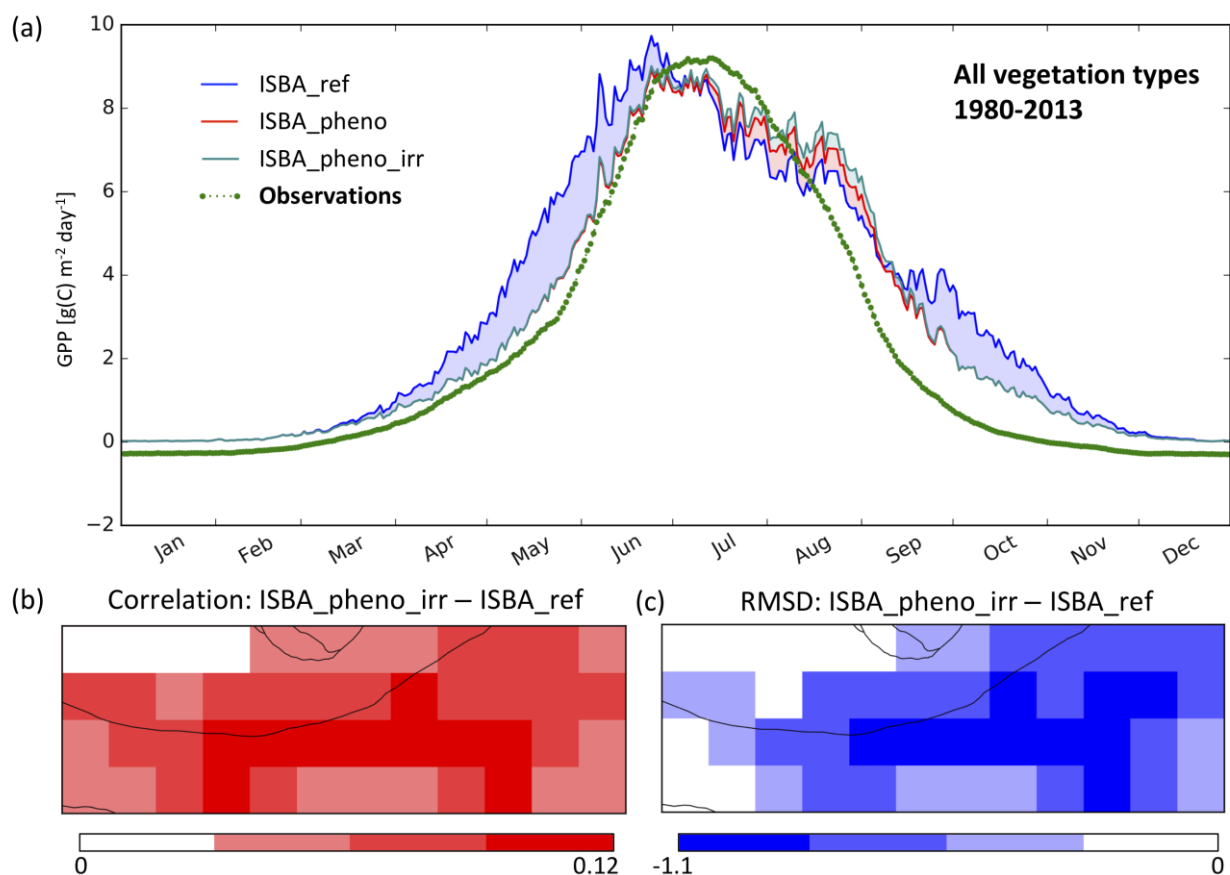


**Figure 8 – Seasonal variation of mean daily GPP values (gC m<sup>-2</sup> d<sup>-1</sup>) in the most densely irrigated part of Nebraska (Fig. 1e) from 1980 to 2013 (a) as derived from the reference simulation ISBA\_ref (blue line), ISBA\_pheno (red line), ISBA\_pheno\_irr (cyan) and observations (green dotted line). Temporal correlation (b) and RMSD (c) score difference maps show the added value of the ISBA\_pheno\_irr simulation with respect to ISBA-ref.**

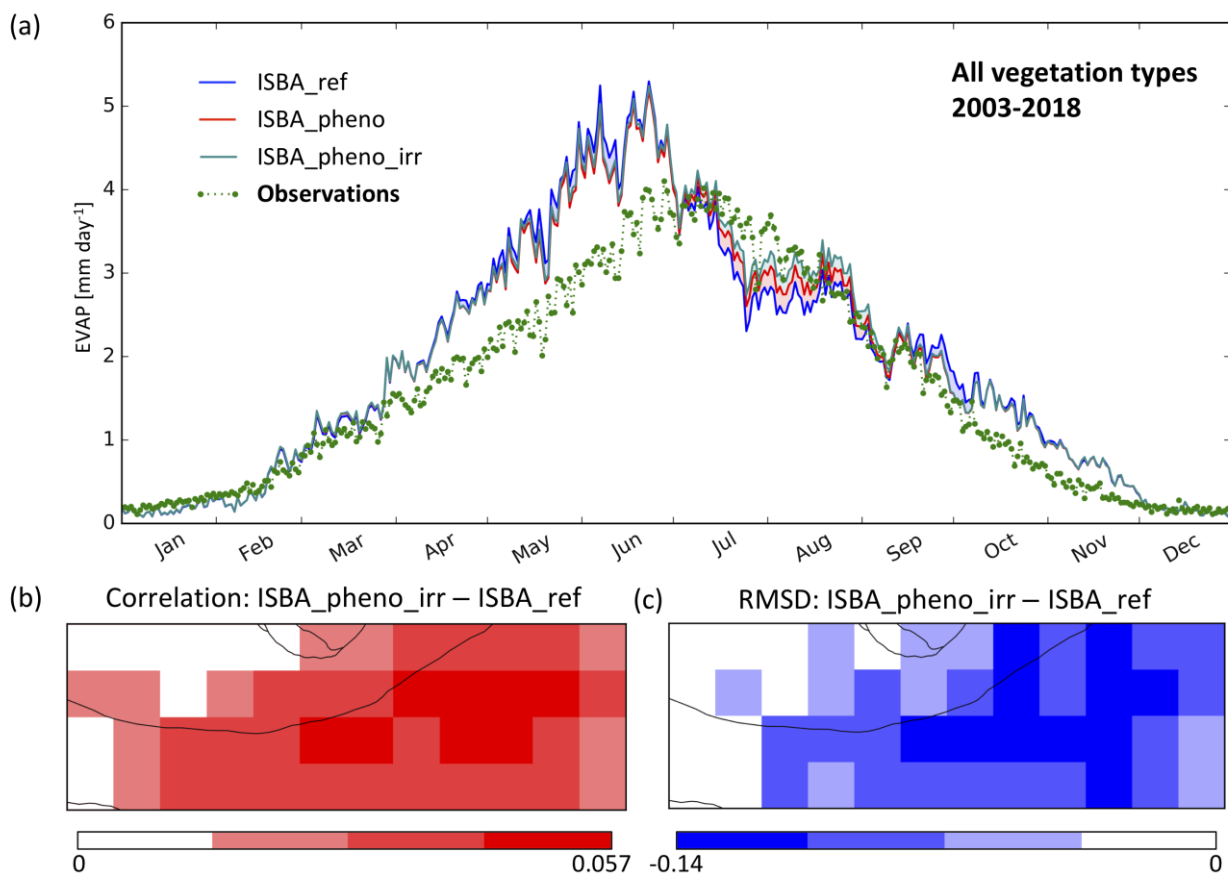


**Figure 9** – Seasonal variation of mean daily evapotranspiration values ( $\text{kg m}^{-2} \text{d}^{-1}$ ) in the most densely irrigated part of Nebraska (Fig. 1e) from 2003 to 2018 (a) as derived from the reference simulation ISBA\_ref (blue line), ISBA\_pheno (red line), ISBA\_pheno\_irr (cyan) and GLEAM observations (green dotted line). Temporal correlation (b) and RMSD (c) score difference maps show the added value of the ISBA\_pheno\_irr simulation with respect to ISBA-ref.

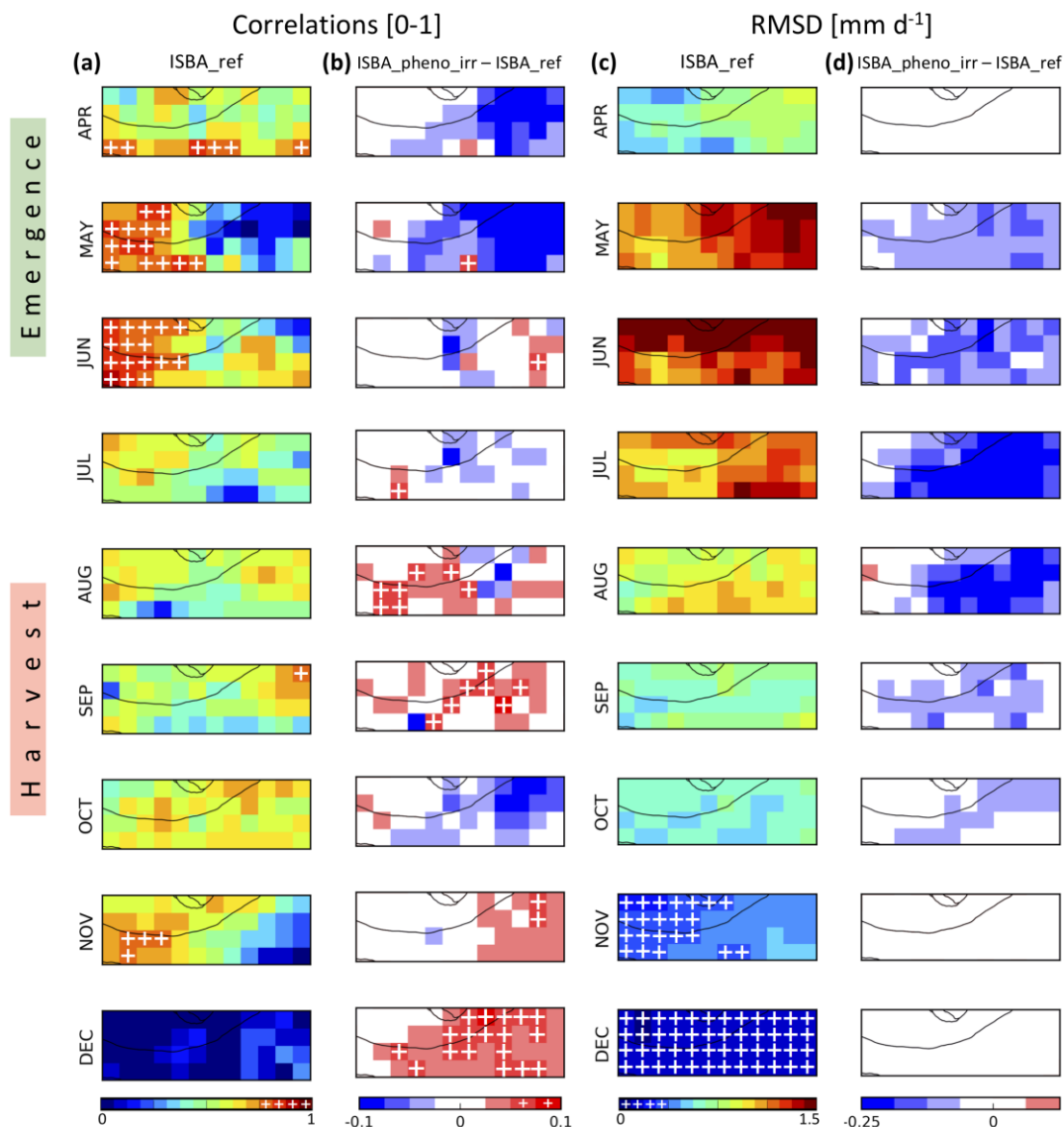


**Figure 10** – Comparison of simulated evapotranspiration with GLEAM evapotranspiration observations in the most densely irrigated part of Nebraska (Fig. 1e) from 2003 to 2018 during the vegetation growing and senescence time period from April to November. Monthly temporal correlation (a, b) and RMSD (c, d) maps are shown for the reference simulation without a representation of irrigation ISBA\_ref (a, c). The added value of the ISBA\_pheno\_irr simulation with respect to ISBA-ref is shown through score difference maps (b, d). ISBA\_ref correlations (RMSD) values larger (smaller) than 0.75 (0.375 mm d<sup>-1</sup>) are indicated by white plus symbols. Correlations differences larger than 0.05 are indicated by white plus symbols.

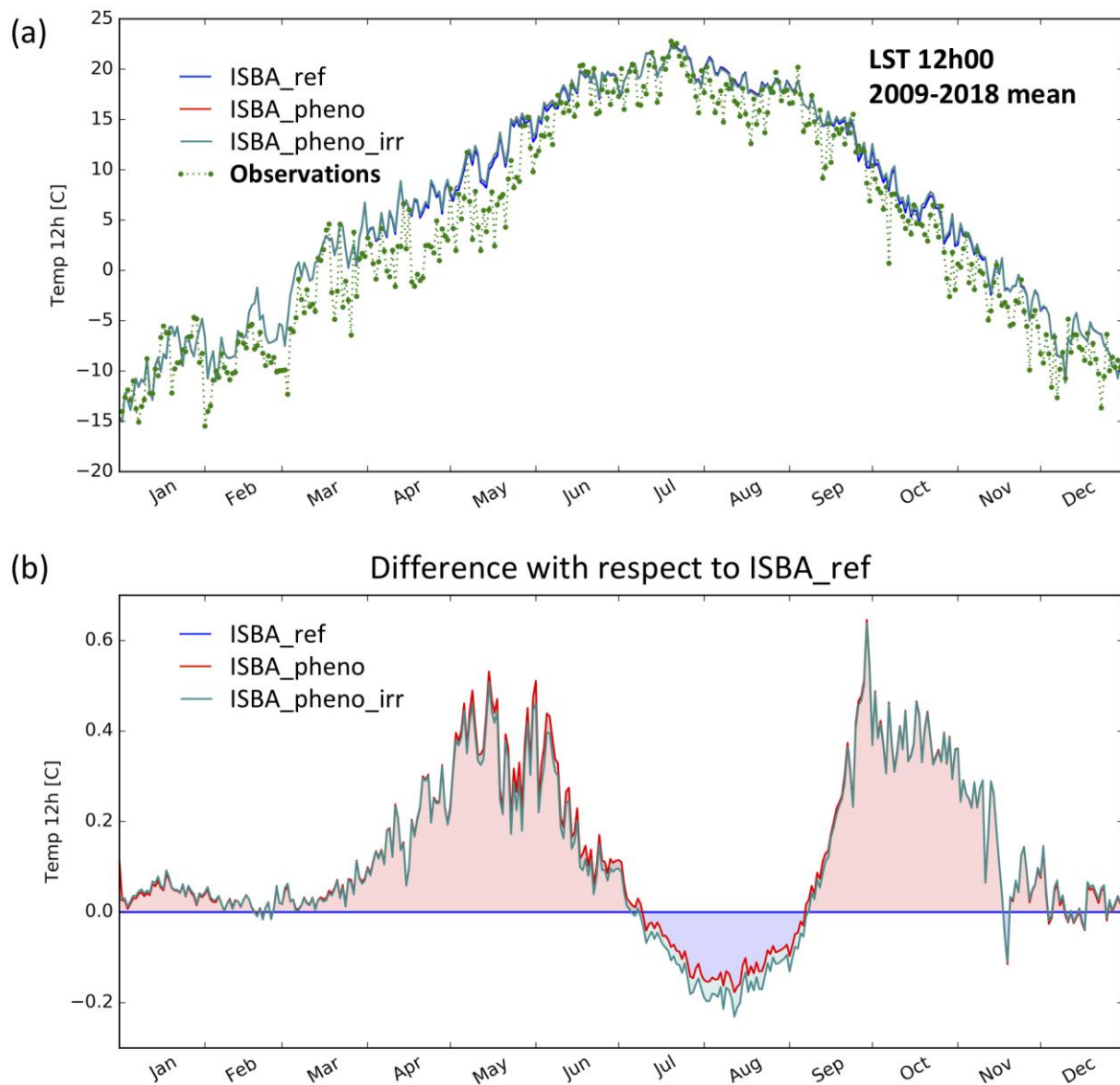


**Figure 11 – Seasonal variation of surface temperature daily values at 12:00 local time (degree C) in the most densely irrigated part of Nebraska (Fig. 1e) from 2009 to 2018 (a) as derived from the reference simulation ISBA\_ref (blue line), ISBA\_pheno (red line), ISBA\_pheno\_irr (cyan) and the CGLS product (green dotted line). The surface temperature differences at 12:00 local time (b) of ISBA\_pheno\_irr and ISBA\_pheno simulations with respect to the ISBA-ref simulations are shown.**

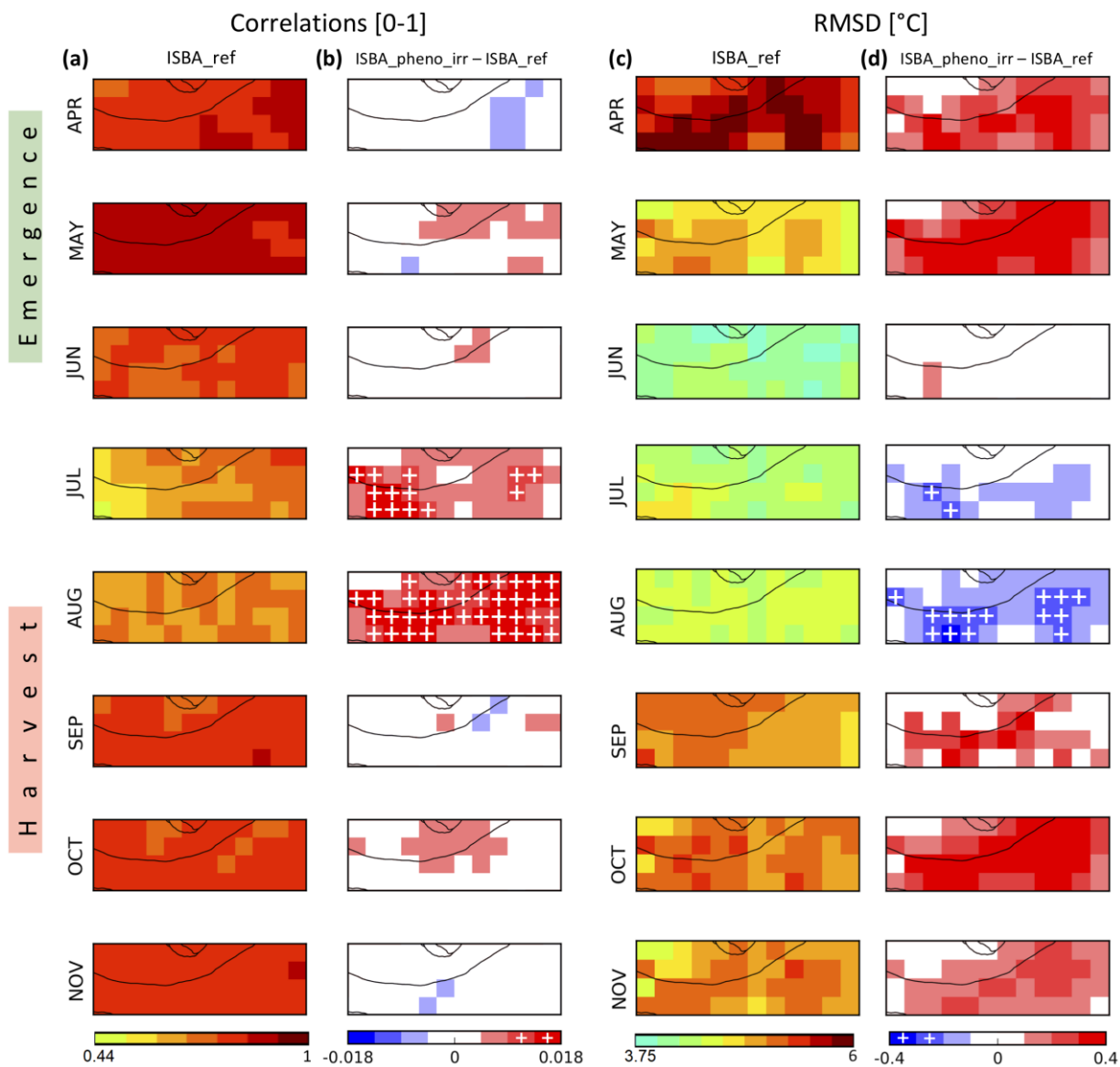


**Figure 12 – Comparison of simulated surface temperature daily values at 12:00 local time with CGLS observations in the most densely irrigated part of Nebraska (Fig. 1e) from 2009 to 2018 during the vegetation growing and senescence time period from April to November. Monthly temporal correlation (a, b) and RMSD (c, d) maps are shown for the reference simulation without a representation of irrigation ISBA\_ref (a, c). The added value of the ISBA\_pheno\_irr simulation**

with respect to ISBA-ref is shown through score difference maps (b, d). Correlations (RMSD) differences larger (smaller) than 0.009 (-0.2°C) are indicated by white plus symbols.